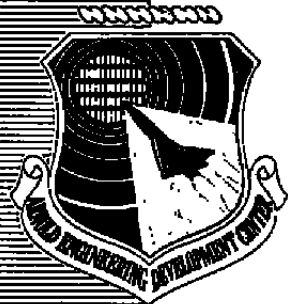


cy.1

**ARCHIVE COPY
DO NOT LOAN**



EXPERIMENTAL STUDY OF STATIC PRESSURE ORIFICE INTERFERENCE

UNIVERSITY OF TENNESSEE SPACE INSTITUTE
TULLAHOMA, TENNESSEE 37388

June 1977

Property of U. S. Air Force
AEDC Library
F40600-77-C-0003

Final Report for Period December 1974 to June 1976

Approved for public release; distribution unlimited.

Property of U. S. Air Force
AEDC LIBRARY
F40600-77-C-0003

Prepared for

DIRECTORATE OF TECHNOLOGY
ARNOLD ENGINEERING DEVELOPMENT CENTER
AIR FORCE SYSTEMS COMMAND
ARNOLD AIR FORCE STATION, TENNESSEE 37389



NOTICES

When U. S. Government drawings specifications, or other data are used for any purpose other than a definitely related Government procurement operation, the Government thereby incurs no responsibility nor any obligation whatsoever, and the fact that the Government may have formulated, furnished, or in any way supplied the said drawings, specifications, or other data, is not to be regarded by implication or otherwise, or in any manner licensing the holder or any other person or corporation, or conveying any rights or permission to manufacture, use, or sell any patented invention that may in any way be related thereto.

Qualified users may obtain copies of this report from the Defense Documentation Center.

References to named commercial products in this report are not to be considered in any sense as an endorsement of the product by the United States Air Force or the Government.

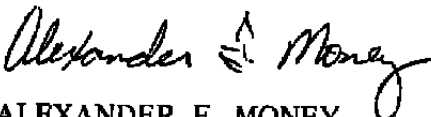
This final report was submitted by University of Tennessee Space Institute, Tullahoma, Tennessee 37388, under contract F40600-75-C-0005, with the Arnold Engineering Development Center, Arnold Air Force Station, Tennessee 37389. Mr. Alexander F. Money was the AEDC technical monitor.

This report has been reviewed by the Information Office (OI) and is releasable to the National Technical Information Service (NTIS). At NTIS, it will be available to the general public, including foreign nations.

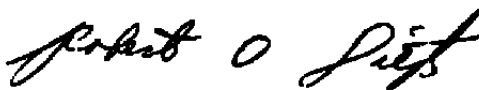
APPROVAL STATEMENT

This technical report has been reviewed and is approved for publication.

FOR THE COMMANDER



ALEXANDER F. MONEY
Research and Development
Division
Directorate of Technology



ROBERT O. DIETZ
Director of Technology

UNCLASSIFIED

REPORT DOCUMENTATION PAGE		READ INSTRUCTIONS BEFORE COMPLETING FORM
1 REPORT NUMBER AEDC-TR-77-57	2 GOVT ACCESSION NO.	3 RECIPIENT'S CATALOG NUMBER
4 TITLE (and Subtitle) EXPERIMENTAL STUDY OF STATIC PRESSURE ORIFICE INTERFERENCE	5 TYPE OF REPORT & PERIOD COVERED Final Report - December 1974 - June 1976	
	6. PERFORMING ORG. REPORT NUMBER	
7 AUTHOR(s) T. H. Moulden, J. M. Wu, F. G. Collins, H. J. Ramm, H. Kuwand, C. I. Wu, and R. Ray	8 CONTRACT OR GRANT NUMBER(s) F40600-75-C-0005	
9 PERFORMING ORGANIZATION NAME AND ADDRESS University of Tennessee Space Institute Tullahoma, TN 37388	10 PROGRAM ELEMENT, PROJECT, TASK AREA & WORK UNIT NUMBERS Program Element 65807F	
11 CONTROLLING OFFICE NAME AND ADDRESS Arnold Engineering Development Center (DYFS) Air Force Systems Command Arnold Air Force Station, TN 37389	12 REPORT DATE June 1977	
	13 NUMBER OF PAGES 82	
	14 MONITORING AGENCY NAME & ADDRESS (if different from Controlling Office)	
		15 SECURITY CLASS. (of this report) UNCLASSIFIED
		15a DECLASSIFICATION DOWNGRADING SCHEDULE N/A
16 DISTRIBUTION STATEMENT (of this Report) Approved for public release; distribution unlimited.		
17 DISTRIBUTION STATEMENT (of the abstract entered in Block 20, if different from Report) <div style="text-align: center; font-size: 2em; font-family: cursive;">2 orifices</div>		
18 SUPPLEMENTARY NOTES Available in DDC		
19 KEY WORDS (Continue on reverse side if necessary and identify by block number) Reynolds number transonic flow scaling boundary layer pressure orifice		
20. ABSTRACT (Continue on reverse side if necessary and identify by block number) Experiments have been performed to evaluate the measurement error in a pressure orifice of diameter of the same order as the boundary layer thickness, and to investigate the disturbance created in the flow downstream of the orifice. It is shown that for small orifice depths the downstream disturbance is small but the flow in the orifice is quite strong. For larger orifice depths the downstream disturbance increases and the measurement error tends to a constant value.		

UNCLASSIFIED

PREFACE

This research was conducted by The University of Tennessee Space Institute, Tullahoma, Tennessee, under sponsorship of the Arnold Engineering Development Center (AEDC), Air Force Systems Command, under Air Force Contract F40600-75-C-0005. The work covers the period December 1974 to June 1976. The Program Element was 65807F. Mr. Alexander F. Money was the AEDC technical monitor for this contract. The principal investigator of this work was Dr. T. H. Moulden. Messers. J. M. Wu, F. G. Collins, H. J. Ramm, H. Kuwano, C. I. Wu, and R. Ray of UTSI also participated in this project and the writing of this report. The objective of the experimental study reported herein was to determine the effect on mean flow and skin friction drag, of model surface irregularities under very thin, fully developed, turbulent boundary layers in compressible transonic flow. Although the objectives were not fully met, the results indicate trends which will be useful in future investigations of this type.

The reproducibles used in the publication of this report were supplied by the authors.

TABLE OF CONTENTS

	Page
I. Introduction.....	7
II. The Test Environment.....	11
III. The Single Orifice Study.....	25
IV. The Multiple Orifice Study.....	39
V. Some Analysis of the Downstream Boundary Layer....	48
VI. Wall Pressure Fluctuations.....	62
VII. General Comments and Relevance of Study.....	75
VIII. Concluding Statement.....	77
References.....	79
Notation.....	81

LIST OF FIGURES

Figure No.	Page
1. The Basic Tunnel Configuration (see Reference 1).....	12
2. The Reference Flat Plate Boundary Layer (after Reference 2).....	13
3a. The Single-Hole Model.....	14
3b. Schematic of Single-Hole Model Arrangement in Tunnel.....	15
4. The Multi-Hole Model.....	17
5. Diagram of the Model Block Showing the Static Pressure Tap Distribution.....	19
6. Instrumentation for Wall Pressure Fluctuation Study.....	21
7. Power Spectral Density Function on a 20 K Bandwidth..	23
8. Measured RMS Pressure Along Working Section. $M_\infty \sim 0.6$	24
9. Effect of 3" Diameter Hole on the Boundary Layer Thickness Downstream of Hole. $M_\infty = 0.8$ $P_t = 26.4$ psia.....	27
10. Velocity Profiles for the Same Conditions as Shown in Figure 9.....	28
11. Static Pressure Distributions Over the Model Centerline ($b = 0$).....	29
12. Effect of Hole Depth on Velocity Profile. $M_\infty = 0.8$ $P_t = 26$ psi Hole Diameter = 3".....	32
13. Static Pressure Distributions on the Piston Surface with Different Hole Depths.....	33
14. Static Pressure Distributions on the Piston Surface with Nearly Constant h/d Ratio (≈ 2.8).....	35
15. Effect of Hole Diameter on Mean Pressure.....	36
16. Dimensionless Pressure Error Against Reynolds Number.....	37

LIST OF FIGURES (Continued)

Figure No.		Page
17.	Hole Configurations for Various Multi-Hole Tests. The hole H1 is at the center of the block and is located at the 40" station on the tunnel centerline.	40
18.	Pressure Distribution on Orifice Floor for Differ- ent Multi-Hole Configurations.....	41
19.	Static Pressure Distributions Along the b = ± 3.25-inch Lines.....	43
20a.	Velocity Profiles, at x = 42.8", Behind Various Multi-Orifice Configurations.....	45
20b.	Continued.....	46
21.	Velocity Profiles at x = 42.8 inches with h/d = 2.8. Single Orifice Study.....	47
22a.	The Disturbed Mean Velocity Profile.....	49
22b.	The Distorted Mean Velocity Profile in Law of the Wall Coordinates.....	50
23a.	Mean Velocity Profiles at Three Different Locations with d = 1 inch and h = 2.83 inches.....	52
23b.	Mean Velocity Profiles at x = 42.8 inches with Nearly Constant h/d Ratio (≈2.8).....	53
23c.	Mean Velocity Profiles at x = 42.8 Inches with Different Hole Depths of 3-Inch Hole Diameter.....	54
24.	Oil Flow Pattern for the Three-Inch Orifice. Flow towards the top right-hand corner.....	55
25.	Diagram of Flow Taken from the Photograph of Figure 24.....	56
26.	Typical Schlieren Photograph of Flow Over 3-Inch Diameter Hole with h/d = 2.84.....	58
27.	Calculated Velocity Profiles for Flow Over a Two- Dimensional Cavity.....	60
28.	The Miniature Pressure Transducer.....	63

LIST OF FIGURES (Continued)

Figure No.	Page
29. Block Diagram of Instrumentation	63
30. Variation of RMS Wall Pressure Fluctuation with Transducer Diameter. After Willmarth(18).....	66
31. The Correlation Coefficient at the Flat-Plate.....	68
32. The Correlation Coefficient behind Orifice.....	69
33. Comparison of Correlation Functions.....	72
34. Calculated Boundary Layer Thickness as a Function of Reynolds Number at $M_\infty = 1.0$	76

I. INTRODUCTION

It has been known for some time that at transonic speeds there can be a significant scaling effect between tests conducted at wind tunnel Reynolds numbers and full-scale. In view of this situation there has been a strong move to establish high Reynolds number test facilities, in particular, there have been studies related to HIRT and to the cryogenic facility. In general terms, the physical dimensions of these proposed tunnels are of the same order as those of existing facilities, with the increased Reynolds number being obtained by changes in either fluid pressure or temperature. This implies that the boundary layer developing over the model surface will be comparatively thin in physical dimensions.

One pertinent measurement to be made in a wind tunnel test is the distribution of static pressure over the model surface. Within the confines of present day measurement techniques, the static pressure will be determined by means of an orifice located on the model surface and connected to a pressure transducer. The model size limitations usually dictate that the pressure transducer must be located outside the wind tunnel. It is standard practice for the orifice hole diameter to be on the order of 0.02 inches, where this diameter is selected, in part, to give adequate instrument response time. This latter requirement would be more severe in short run-time blow-down facilities. It can be anticipated that the inclusion of such an orifice in the model surface will have certain detrimental features in

relation to the model flow. Among these will be included a measurement error when the pressure gradient is large, a possible measurement error if Helmholtz resonance occurs within the tube system and other errors when the boundary layer and orifice diameter are of the same order. The present study pertains to the latter problem areas which can be identified as follows.

Consider the situation wherein the boundary layer flowing over a surface encounters an orifice whose diameter is of the same order as the thickness of the viscous layer. Then it is evident that there are certain parallels between the ensuing flow and that associated with a base configuration. It is well known that considerable reduction in pressure occurs in a base flow region. This analogy only refers to the upstream lip of the orifice. Once the flow has negotiated this upstream lip it is clear that the downstream lip of the orifice amounts to a forward-facing step. In short, the orifice has some of the characteristics of a deep cavity flow. The fact that the orifice is circular will add a strong three-dimensional component to the flow with possible trailing vortex systems being established. These deliberations will lead to the expectation that a large pressure gradient would exist in the streamwise direction across the orifice. This is particularly true for the region within one diameter below the model surface but this pressure gradient will be attenuated through the tube connecting the orifice and the transducer. As a result of this flow situation the pressure sensed at the transducer face would not be the same as that associated with the flow over the model surface in the absence of the orifice.

At the same time the boundary layer developing downstream of the orifice would bear little resemblance to that of the undisturbed flow. There are two reasons for this. In the first instance, the boundary layer velocity profile would be strongly perturbed due to its excursion into the mouth of the orifice. The situation is compounded by the presence of a distorted pressure field established by flow in the orifice. Also, if the tube system resonates then the whole flow would be unsteady. The presence of this distorted flow field could deteriorate the quality of measurement at a similar orifice located somewhat downstream. The combined effect resulting from an array of such orifices may be sufficient to interact with gross features of the flow such as the shock wave location at transonic speeds.

It should be noted that orifice locations in the immediate vicinity of a stagnation point may be subject to an interaction with laminar boundary layers. In this case it is possible that premature transition would be initiated. This is an important area for study but will not feature in the present deliberations.

The present work will concern itself with the fundamental study of the interaction of a turbulent boundary layer and a surface static pressure orifice. The problem has been simplified to treat only flows for which the external pressure is constant. This simplification does not anticipate that pressure gradient effects can be neglected.

The work is in two main areas. The first part of the study deals with the flow in and downstream of a single orifice where the parameters varied were the hole diameter to boundary layer thickness ratio and the hole diameter to depth ratio. In these tests the static pressure inside and around the orifice was measured along with pertinent boundary layer profiles. The second phase of the study related to the mutual interference between adjacent holes.

All tests were conducted in the Mach number range between 0.6 and 0.9 and the tunnel total pressure in the range 20 to 27 psi, giving a Reynolds number range of 0.49×10^6 to 0.8×10^6 /inch. The geometric parameters and their range of variation will be discussed along with the model geometry in the next section.

II. THE TEST ENVIRONMENT

The tests were conducted in the UTSI Transonic Flow Facility which has been described in previous publications (Ref. 1). The working section of the tunnel is twelve inches square and 140 inches long. The floor of the facility, which is used as the test model, has a boundary layer removal device just downstream of the nozzle exit (see Fig. 1). The top wall is perforated to allow mass relief into a plenum chamber and allows testing at transonic speeds with minimal wall interference. In the tests conducted for the present study the centerline of the simulated orifice was located 41 inches downstream of the boundary layer removal device. All streamwise locations are referenced to this leading edge.

Under the conditions of free-stream Mach number and total pressure adopted in this study, the boundary layer thickness at the forty-inch location was a little less than one inch. The reference flat-plate boundary layer is displayed on Figure 2 (see Ref. 2). This distribution of boundary layer quantities will be used to non-dimensionalize subsequent data so that such ratios as d/δ^* will relate to this undisturbed flat-plate boundary layer. In this way any upstream influence that the simulated orifice may produce is not included in the reference conditions.

The simulated single orifice model is shown in Figure 3, while the geometry parameters are summarized in Table I. The

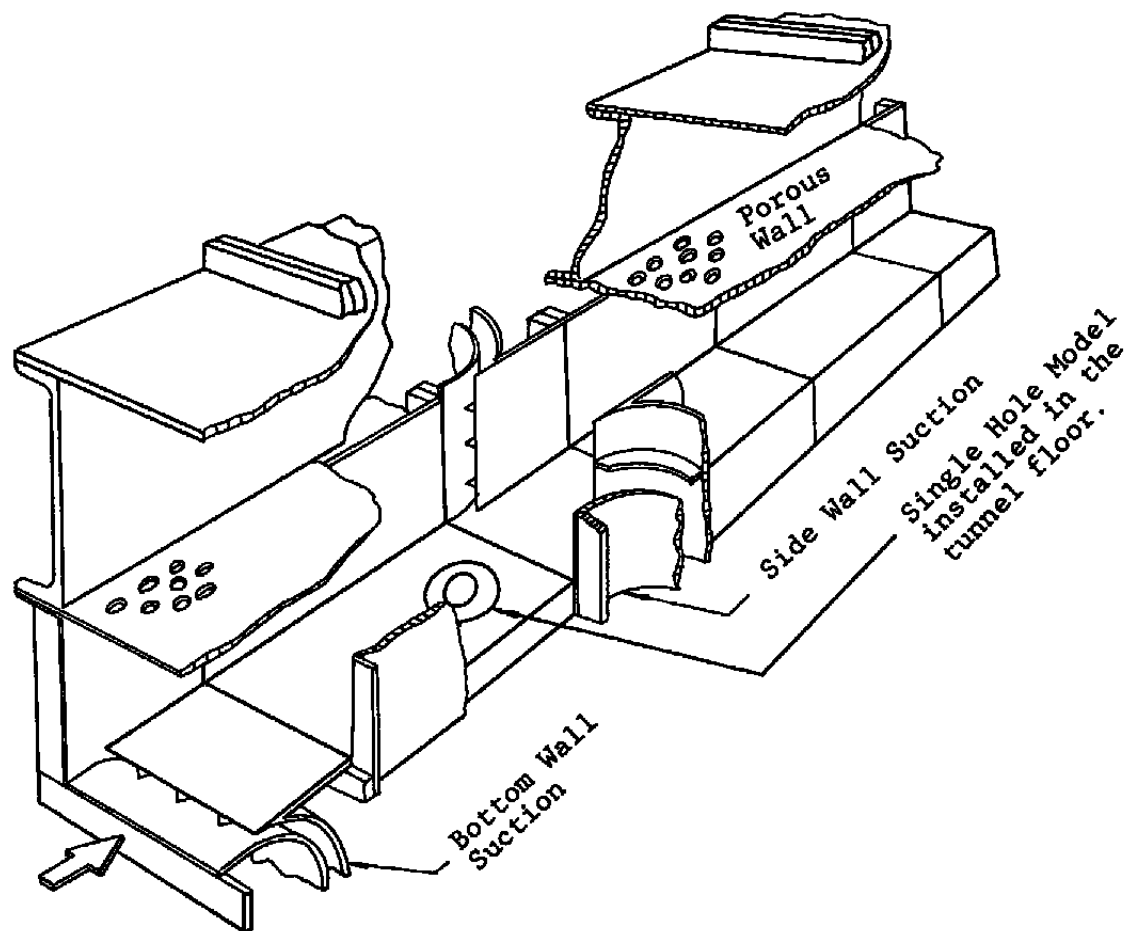


Figure 1. The Basic Tunnel Configuration (see Reference 1).

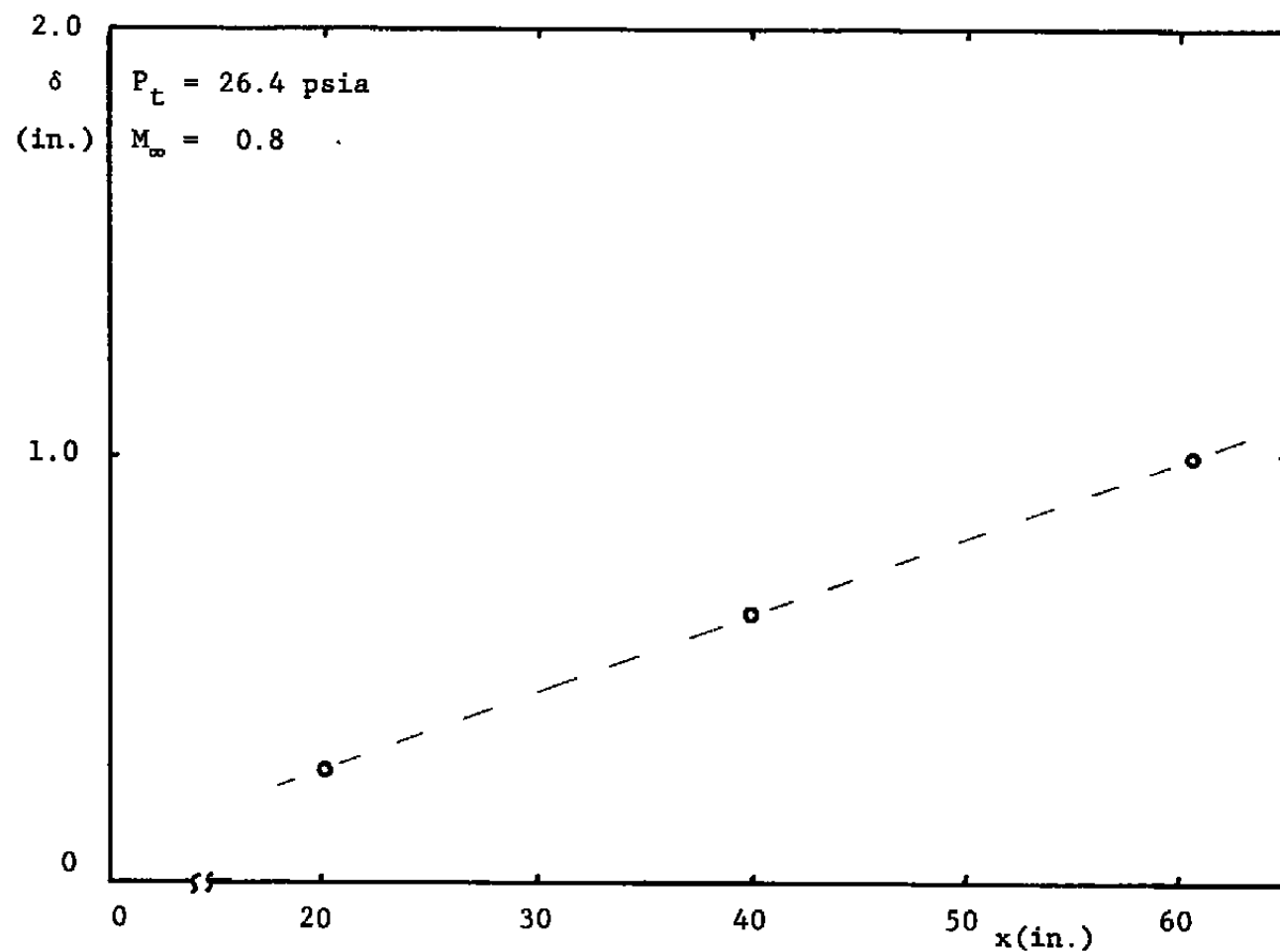


Figure 2. The Reference Flat Plate Boundary Layer (after Reference 2).

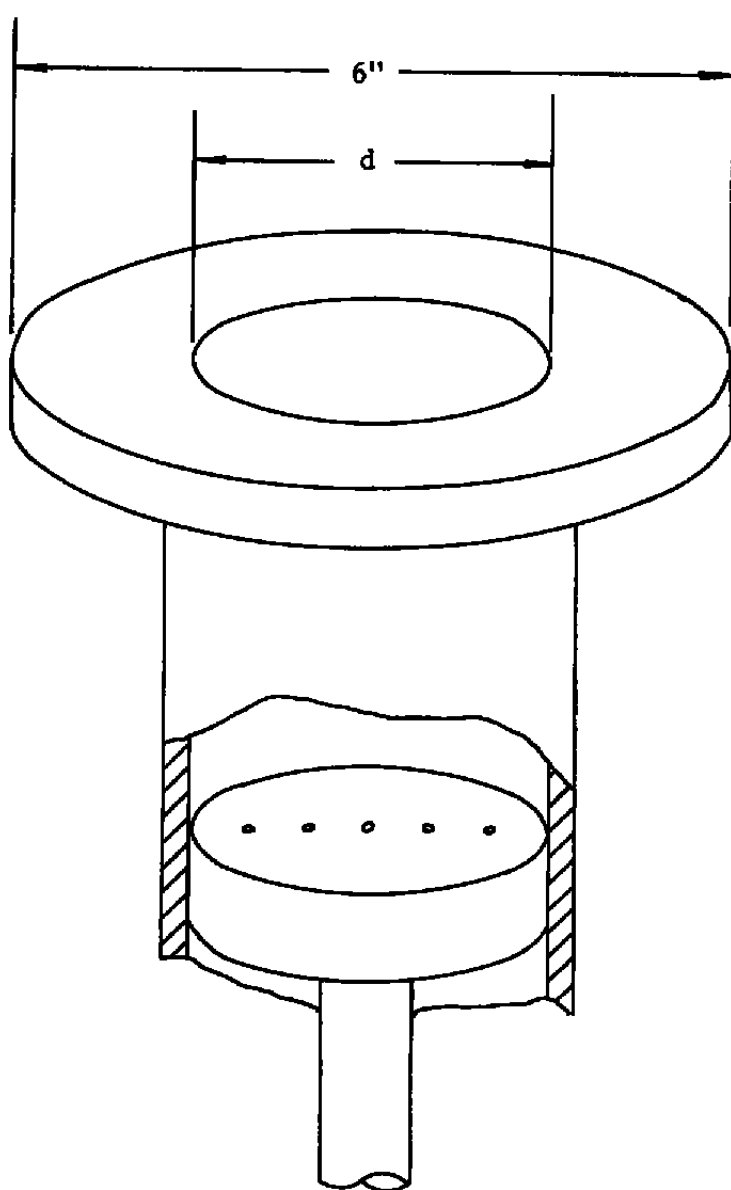


Figure (3a). The Single-Hole Model.

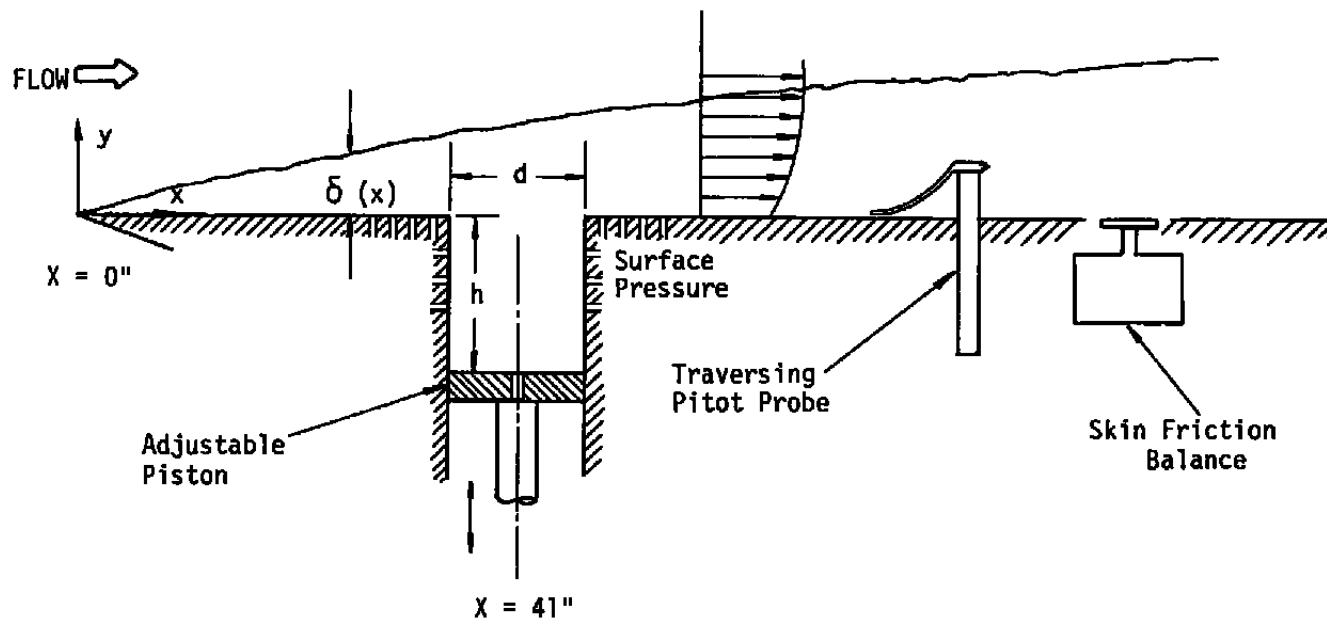


Figure (3b). Schematic of Single-Hole Model Arrangement in Tunnel.

TABLE 1

Geometric Parameters of Single Hole Models Studied.

h(in.)	d(in.)	h/d
8.53	3	2.84
3	3	1
0.5	3	0.17
2.83	1	2.83
1.38	0.5	2.76

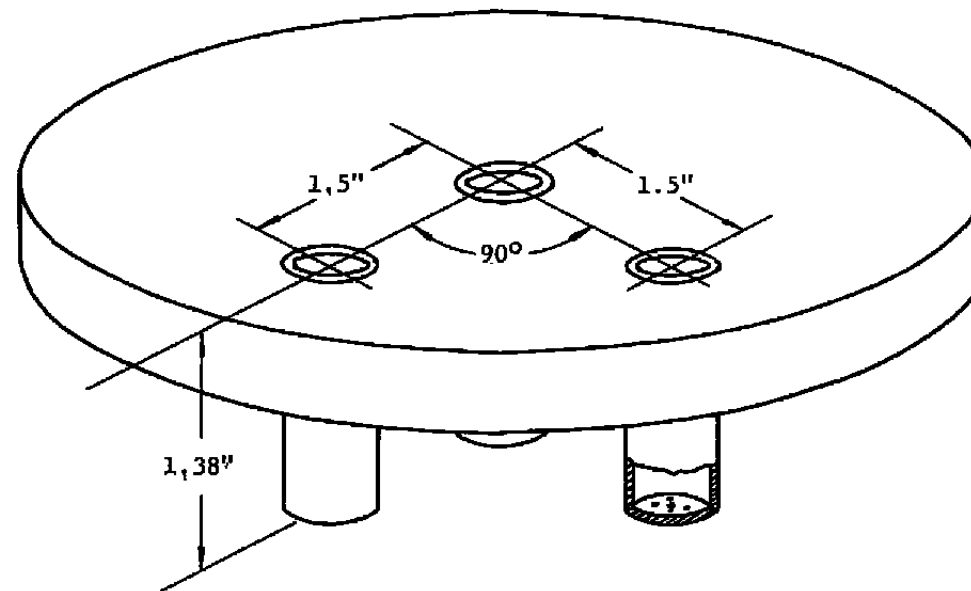


Figure 4. The Multi-Hole Model.

multiple-hole model tested is shown in Figure 4. Each model is mounted on a six-inch diameter plate which bolts directly to the tunnel floor. In the case of the multiple-hole model, it was possible to rotate the mounting plate in order to vary the angular spacing between the adjacent holes. Figure 5 shows the array of static pressure taps surrounding the simulated orifice model. These pressure taps were connected to a pressure transducer via a scanivalve attachment. Boundary layer surveys were also made at various locations downstream of the hole.

The largest orifice model tested was three inches in diameter and was equipped with a piston mechanism so that the depth to diameter ratio could be varied. The maximum depth of piston travel was 8.5 inches giving a depth to diameter ratio of 2.8; the purpose of this test being to establish the sensitivity of the measured pressure to the orifice geometry. The geometry adopted would apply most directly to situations where the pressure transducer was mounted in the model in close communication with the external stream. It has been shown (Ref. 3) that the spectrum of the surface pressure fluctuations is critically dependent upon the lack of flushness in the transducer mounting. While the present study is more concerned with mean pressure measurement there is still merit in assessing the sensitivity to orifice geometry. Results would also show in crude terms the attenuation in pressure gradient along the orifice-transducer connecting tube. In no sense could such a configuration be utilized to measure the spectral properties of the wall pressure fluctuations

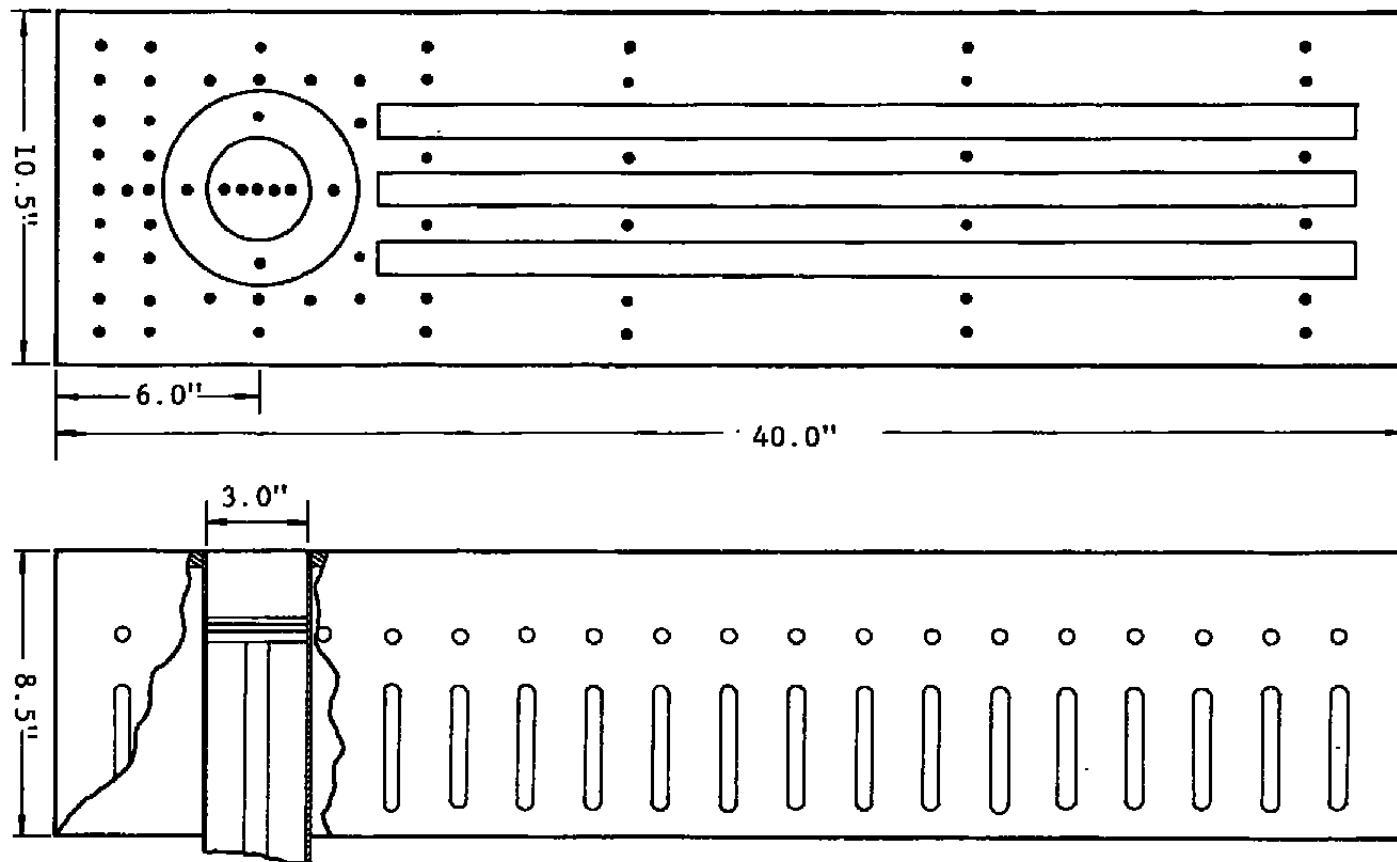
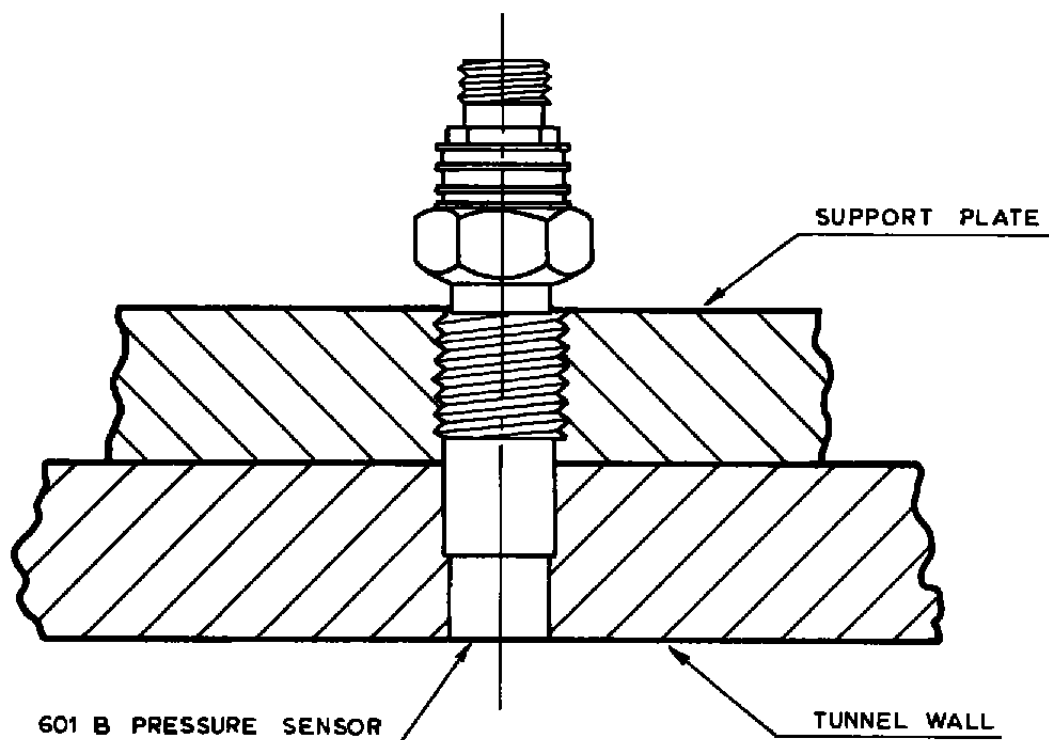


Figure 5. Diagram of the model block showing the static pressure tap distribution.

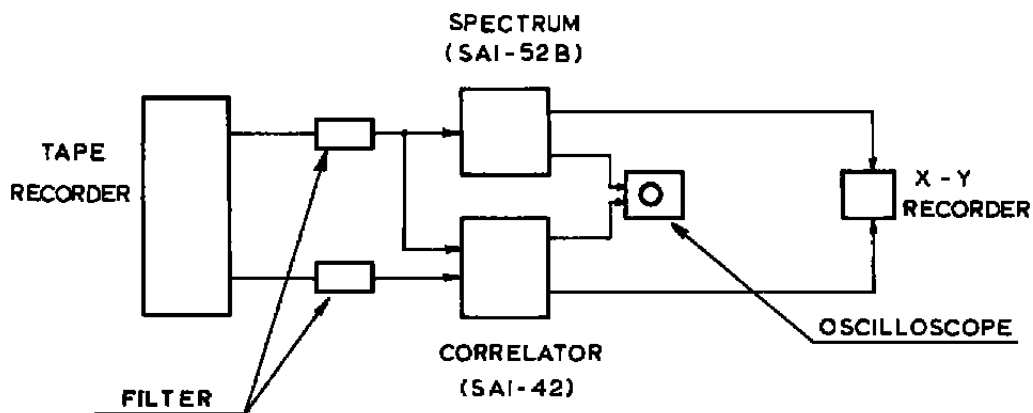
due to the dampening of the high frequency content by the connecting tube. For the assessment of the mean pressure error, however, this is of little import.

A subsidiary part of the experimentation was concerned with attempting to establish some understanding of the turbulent structure modification brought about by the orifice interaction. The study was restricted to measurements of wall pressure fluctuations and to discussion of their properties. In particular it would be of interest to determine any changes that occur in the spectral distribution at a given point as the cavity geometry is changed. It can be anticipated that if the orifice suffered a pure resonance then this would be detected as a narrow-band distortion in the spectrum at the resonant frequency. On the other hand, if some additional phenomena is enacted then this may well bring about a broad-band modification to the spectrum. For example Plotkin (Ref. 4) predicts a substantial amplification of the pressure fluctuations under a shock-wave boundary-layer interaction as a consequence of the shock interaction with the boundary layer turbulence structure.

To make such studies meaningful it is necessary to know the pressure fluctuation characteristics residing in the basic tunnel flow. A cursory evaluation of the tunnel wall pressure spectrum was consequently conducted. To this end a Kistler piezoelectric transducer (Model 601 B) was flush-mounted to the tunnel wall. A diagram of the transducer mounting and the associated analysis equipment is shown in Figure 6.



a) TRANSDUCER MOUNT



b) DATA ANALYSIS

Figure 6. Instrumentation for Wall Pressure Fluctuation Study.

Figure 7 shows the pressure power spectral density function as measured on the tunnel sidewall at approximately the model location. The free-stream Mach number was approximately 0.6 and the free-stream total pressure was 20 psia. The rms wall pressure fluctuation along the tunnel is shown in Figure 8 along with the spread of data over different runs. These results should be taken into consideration when subsequent data is evaluated.

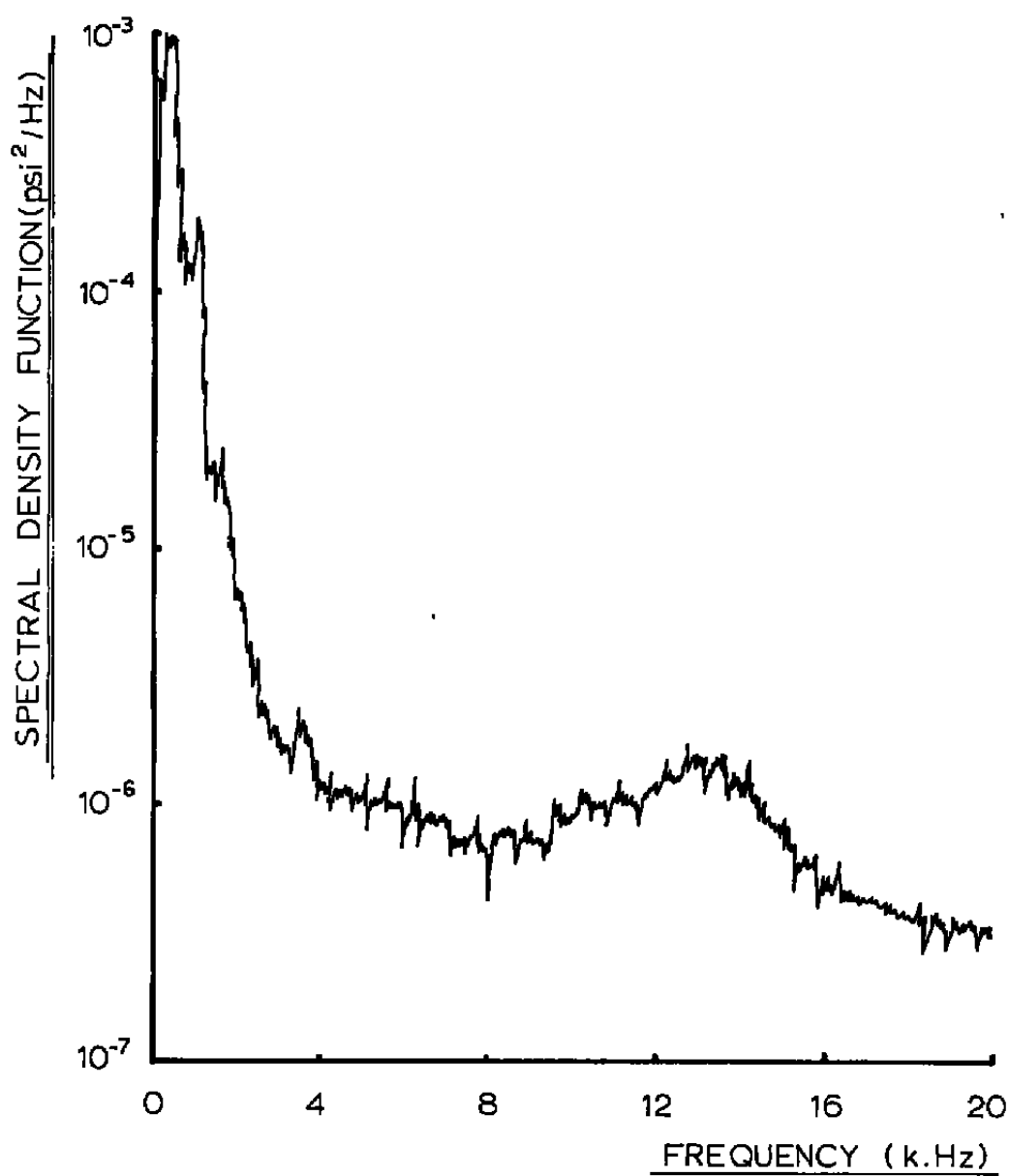


Figure 7. Power Spectral Density Function on
a 20 K Bandwidth.

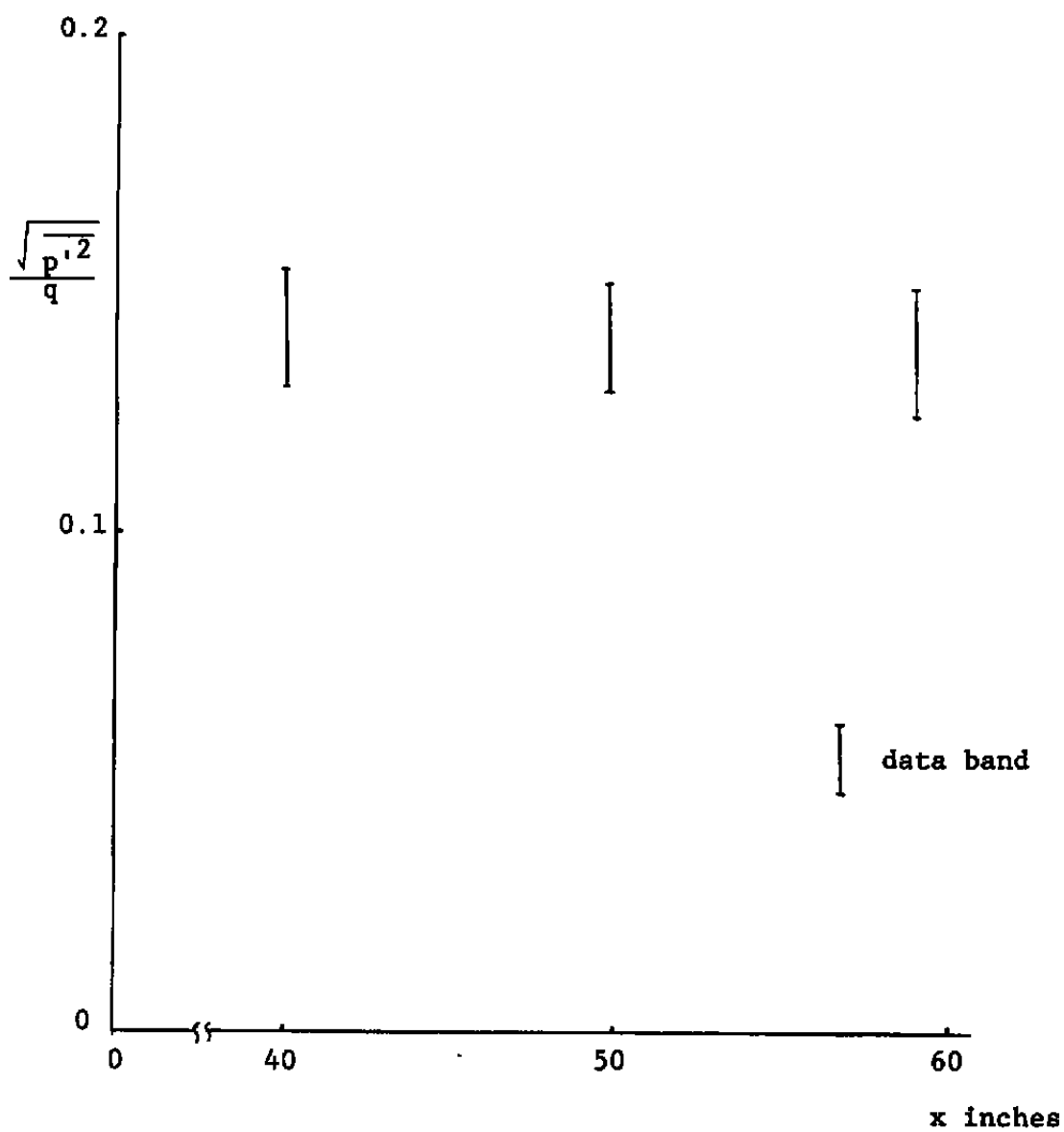


Figure 8. Measured RMS pressure along working section.
 $M_\infty \sim 0.6$.

III. THE SINGLE ORIFICE STUDY

Tests were performed on the single hole model shown in Figure 3 over the Mach number and total pressure ranges shown in Table 2. The tests confirm that the largest diameter holes (relative to the boundary layer thickness) create the largest disturbance. In general terms the disturbance is most readily detected as a distortion of the boundary layer velocity profile directly downstream of the hole location. Figure 9 shows the increase in boundary layer thickness that occurs on the center-line downstream of the 3" hole when the depth to diameter ratio is 1.0. Immediately downstream of the hole (at the 42.8" location) there is little detectable difference in boundary layer thickness over the flat plate values. Further downstream, however, the disturbed boundary layer grows at a much higher rate; the reasons for which become evident from the measured boundary layer profiles (Figure 10). At locations just downstream of the hole (42.8" station) it is found that the major distortion of the velocity profile occurs close to the wall with the external edge of the boundary layer showing little change. Despite this, the wall boundary condition

$$\frac{\partial P}{\partial x} \sim \frac{\partial}{\partial y} \left(\mu \frac{\partial u}{\partial y} \right)$$

must relate the pressure gradient with the profile properties at the wall. There is then, some correspondence between the wall pressures measured as in Figure 11 and the wall region of the velocity profiles. The fact that the wall pressure returns to

TABLE 2

Range of Free-Stream Parameters.

M_{∞}	P_t	h/d
0.65 ~ 0.80	20.0 ~ 26.0	2.84
0.65 ~ 0.80	21.2 ~ 26.3	1
0.65 ~ 0.80	21.2 ~ 26.2	0.17
0.71 ~ 0.84	21.2 ~ 26.9	2.83
0.7 ~ 0.8	21.2 ~ 26.0	2.76

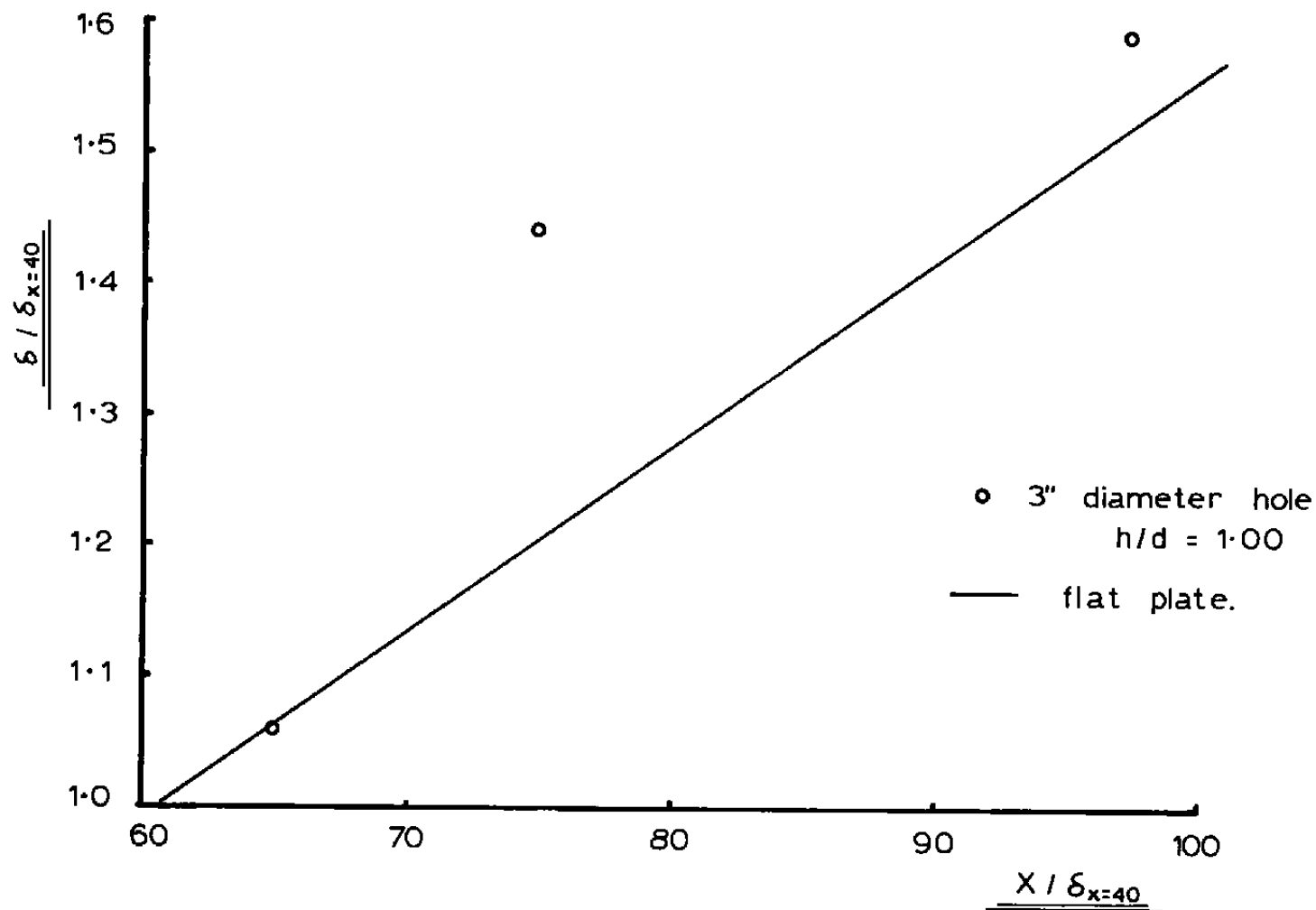


Figure 9. Effect of 3" Diameter Hole on the Boundary Layer Thickness Downstream of Hole. $M_\infty = 0.8$ $P_t = 26.4$ psia

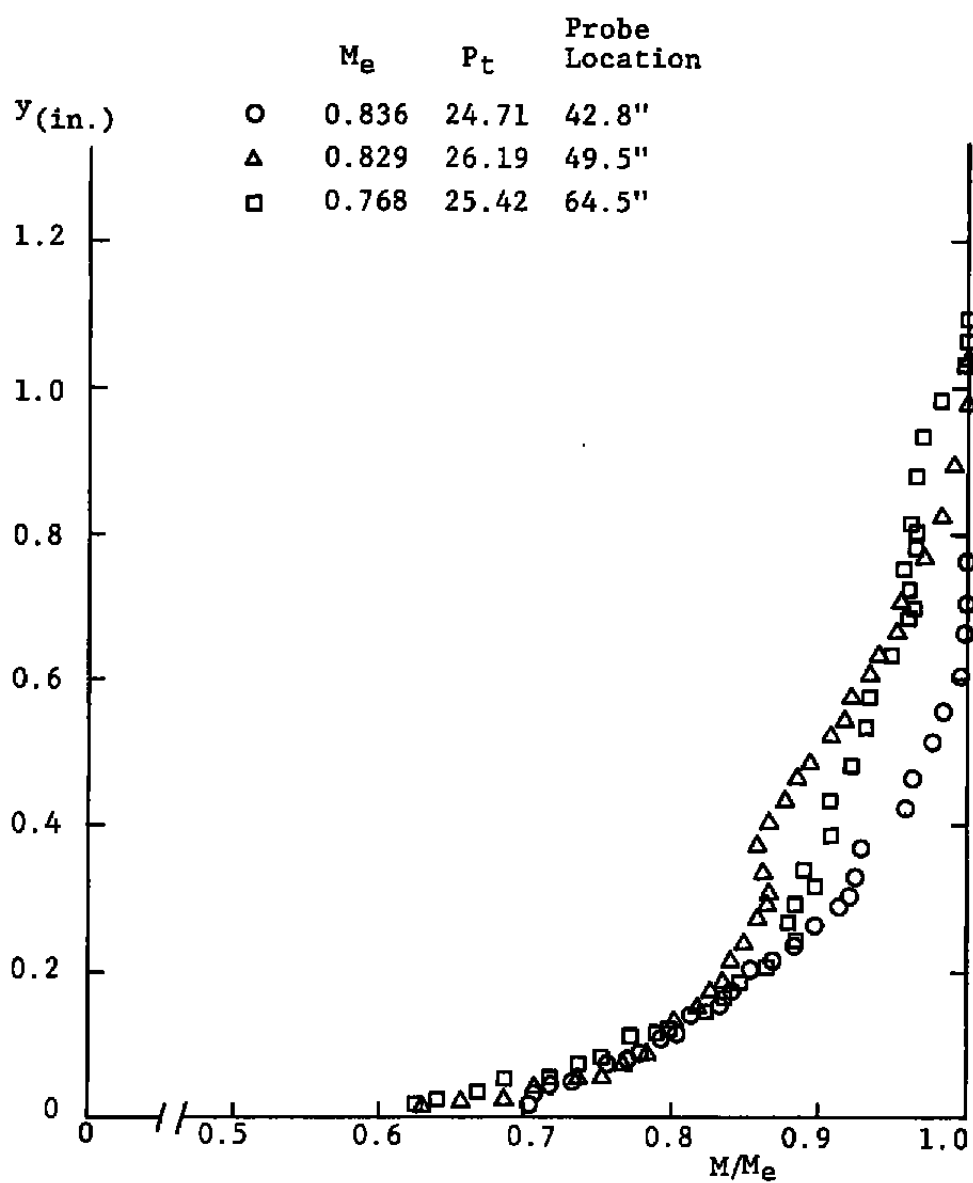


Figure 10. Velocity Profiles for the Same Conditions as Shown in Figure 9.

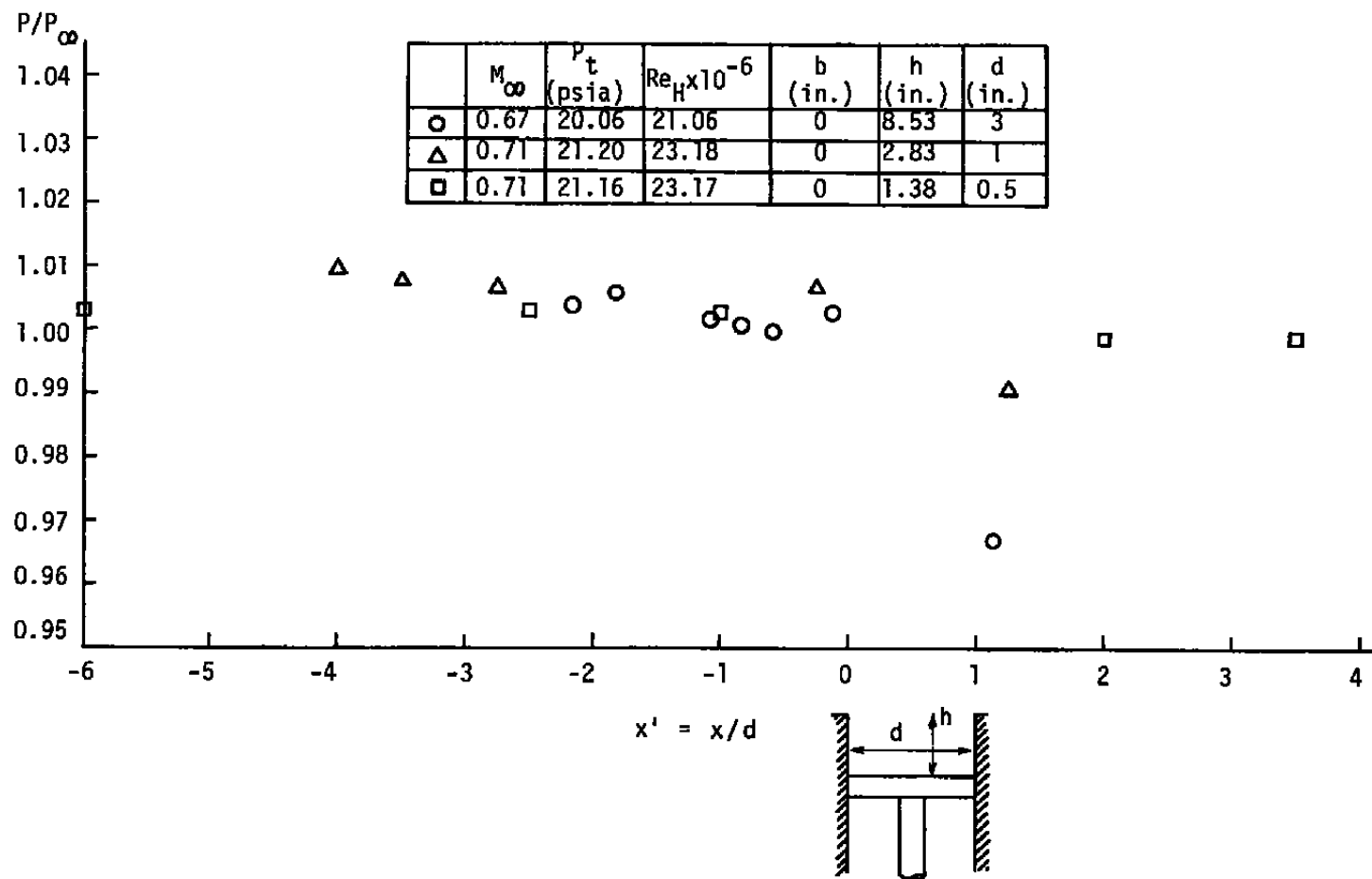


Figure 11. Static pressure distributions over the model centerline ($b = 0$).

the free-stream value very quickly (within two or three hole diameters downstream of the hole centerline) would also require the wall region of the velocity profile to return to equilibrium rapidly. The initial disturbance produced in the flow must, however, be advected with the mean motion within the boundary layer and suffer diffusion due to the local turbulent mixing process. This aspect of the flow is again recorded in the velocity profiles shown in Figure 10. As the flow progresses downstream then the disturbance that was originally observed close to the wall is found to migrate to the outer edge of the boundary layer. At the same time, the inner layer returns to equilibrium very rapidly and the boundary layer thickness increases.

Another important geometric parameter is the hole depth to diameter ratio. With the increased tendency towards miniaturization in all aspects of instrumentation design, it is not unreasonable to suppose that at some future time it will be more usual to have pressure transducers located directly inside the model to improve response time. In such a situation, questions relating to the mounting configuration of the transducer are important and the hole depth to diameter ratio would feature here. It can also be noted that (for low speed flow) Wieghardt⁽⁵⁾ showed a drag maximum when the ratio h/d was about one half. This maxima was attributed to the presence of the sharpest resonance in the flow at this hole geometry.

The two aspects of the orifice interaction problem discussed above are related and a compromise must be established between the measurement error admissible and the extent of downstream disturbance that can be tolerated. Thus, Figure 12 shows the effect of hole depth to diameter ratio on the velocity profiles directly downstream ($x = 42.8''$) of the three-inch diameter hole. It is immediately evident from this figure that the ratio h/d has an important influence on the downstream flow disturbance. Large values of this ratio lead to a large disturbance to the downstream flow. Several additional factors need consideration beside the mean boundary layer velocity profiles. In the first place, the present results are all for a time-averaged pressure (or velocity) measurement and no assessment of a resonance in the orifice has been made. Again, the three-dimensional character of the orifice flow has not been established in any detail.

Figure 13 shows the measured pressure distribution across the piston face for the three-inch diameter orifice. The results break into two groups. For small h/d there exists a large gradient of pressure across the hole and this suggests a vigorous flow into the hole in such configurations. It is difficult to assess the actual pressure levels being simulated and hence the mean pressure error. For larger values of h/d it is seen that the pressure gradient is much flatter since the deep hole attenuates the large disturbances present near the orifice mouth (and shown to be a dominant feature of the low h/d flow).

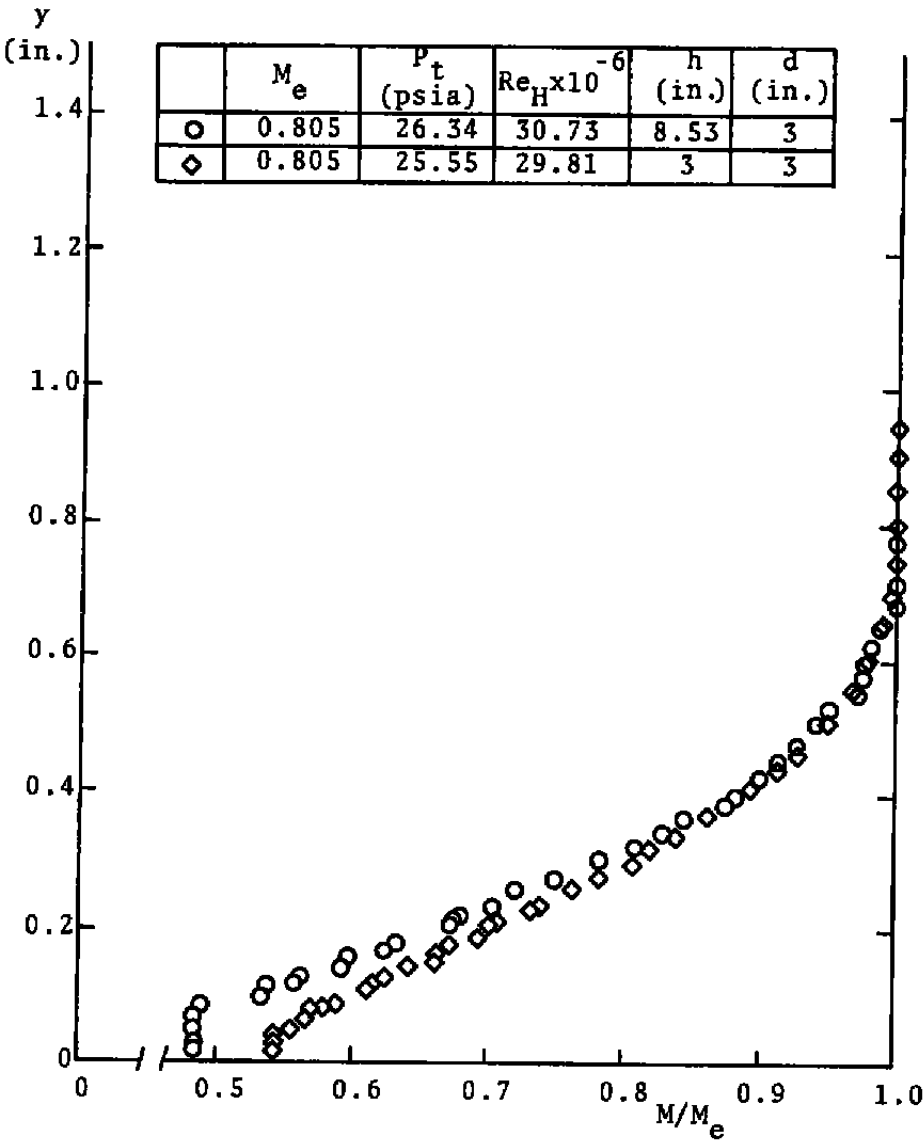


Figure 12. Effect of Hole Depth on Velocity Profile.
 $M_\infty = 0.8$ $P_t = 26$ psi Hole Diameter = 3"

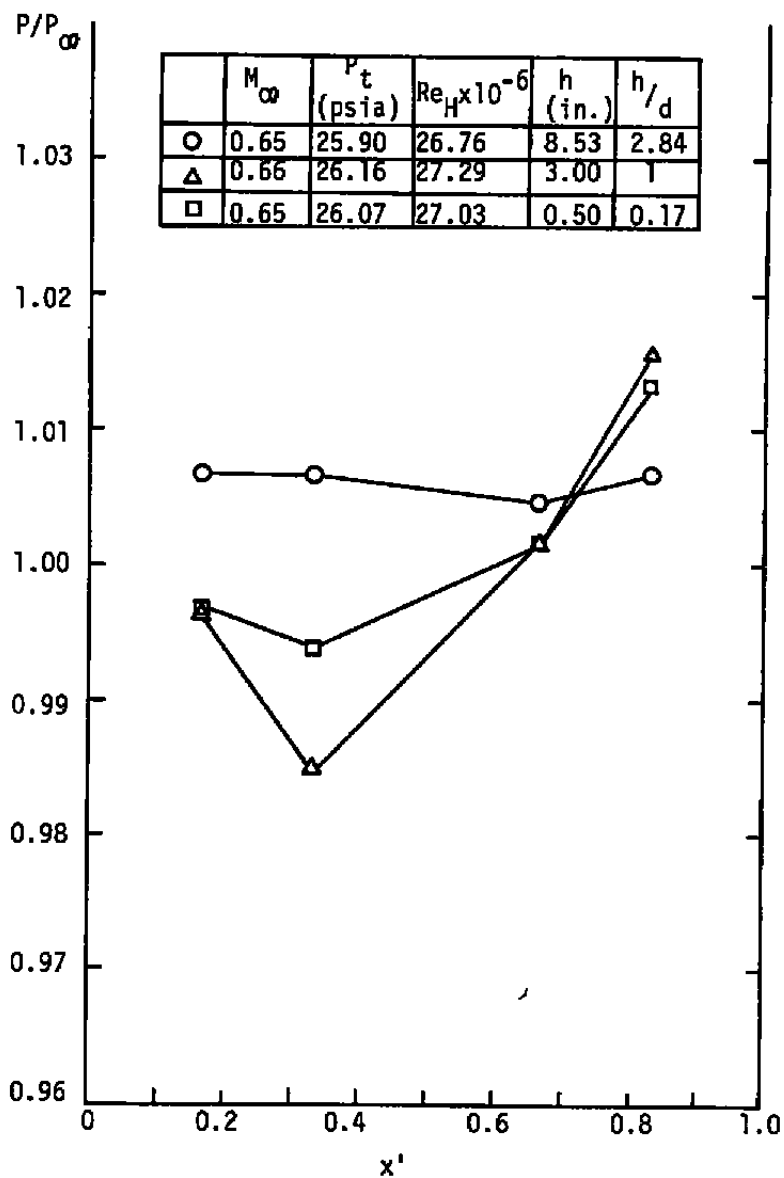


Figure 13. Static pressure distributions on the piston surface with different hole depths.

This result for large h/d is more or less carried over to cases where the ratio d/δ^* is changed with h/d held constant. Thus Figure 14 plots the results for $h/d = 2.8$ while the simulated orifice diameter is changed but the approach boundary layer is unaltered. Now the gradient across the orifice is not too large, but the mean pressure error is a function of the hole diameter--or better to the d/δ^* ratio. An indication of this mean pressure error is shown in Figure 15, but it must be recognized that the establishment of a mean value from the data shown in Figure 14 is somewhat open to interpretation. The results are in conformity with expectation since the mean pressure approaches the free-stream value as the ratio d/δ^* approaches zero. It is also interesting to note that the results indicate a plateau value is reached as the orifice diameter becomes large compared to the boundary layer thickness, but there is no evidence from the present tests to indicate if the same trend continues as the orifice diameter becomes very large. In non-dimensional terms, these results are plotted on Figure 16 where the friction velocity is determined from the undisturbed flat plate boundary layer. Here the results are plotted as the pressure error ($\Delta P = | P_\infty - P_{\text{mean}} |$) divided by the wall shear against a Reynolds number based on hole diameter and wall friction velocity u_τ . Also shown on this figure are the results obtained by Ray⁽⁶⁾ and Shaw⁽⁷⁾ for incompressible flow. Any comparison between the present results and those of Refs. (6) and (7) must allow for the effect of compressibility and the higher Reynolds

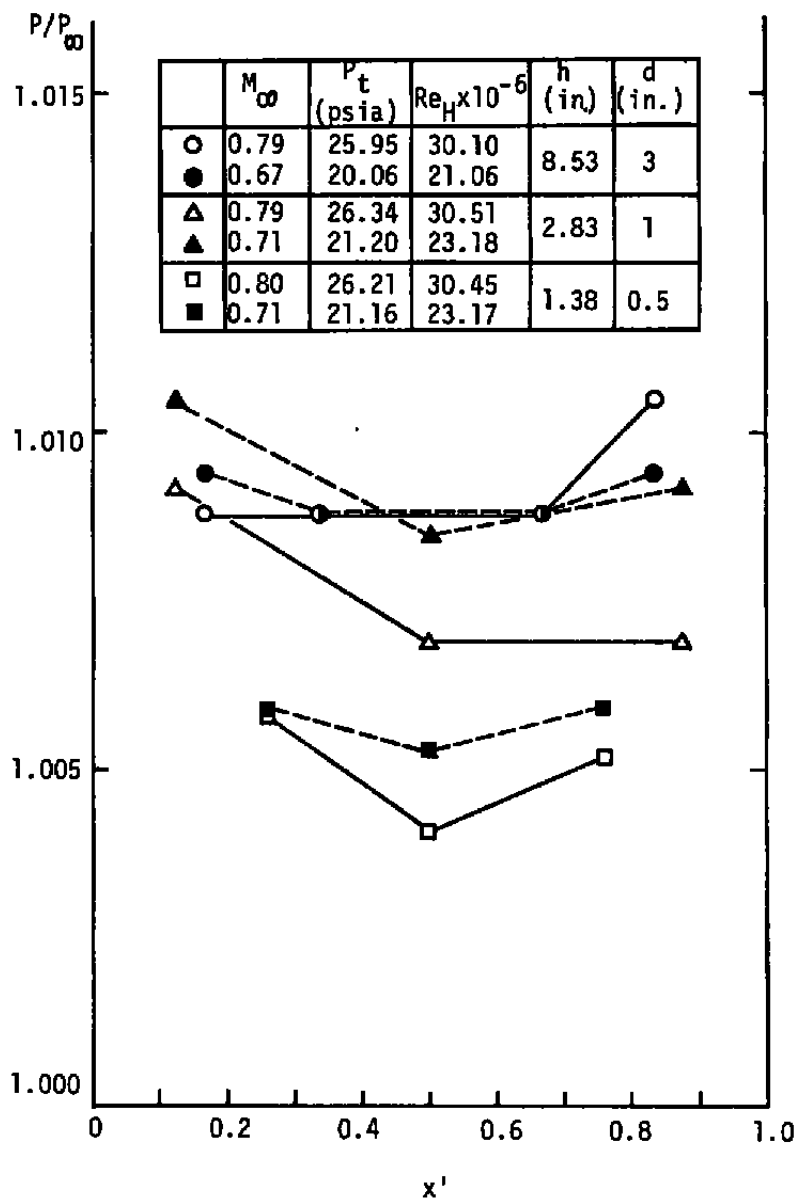


Figure 14. Static pressure distributions on the piston surface with nearly constant h/d ratio (≈ 2.8).

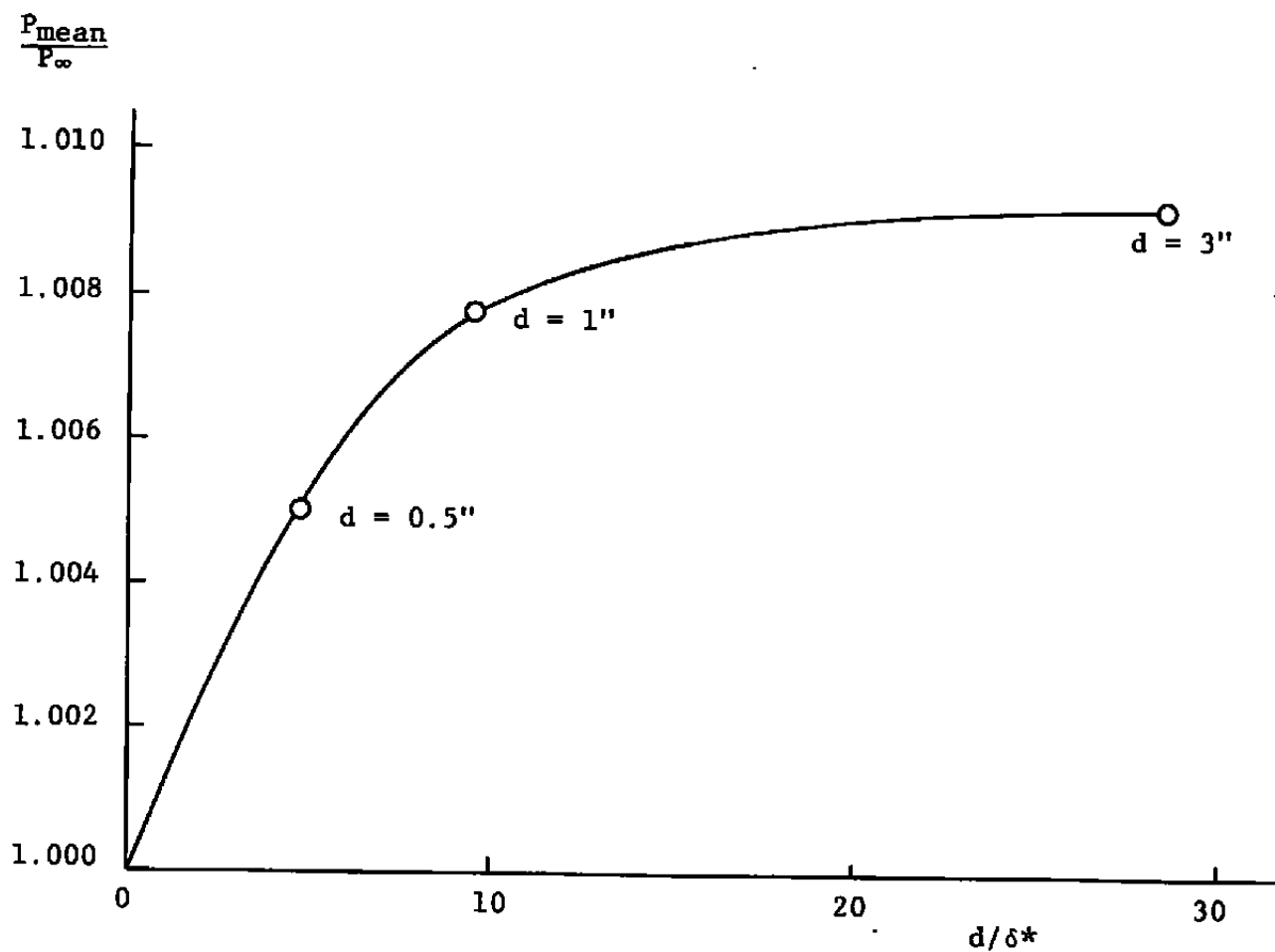


Figure 15. Effect of Hole Diameter on Mean Pressure.

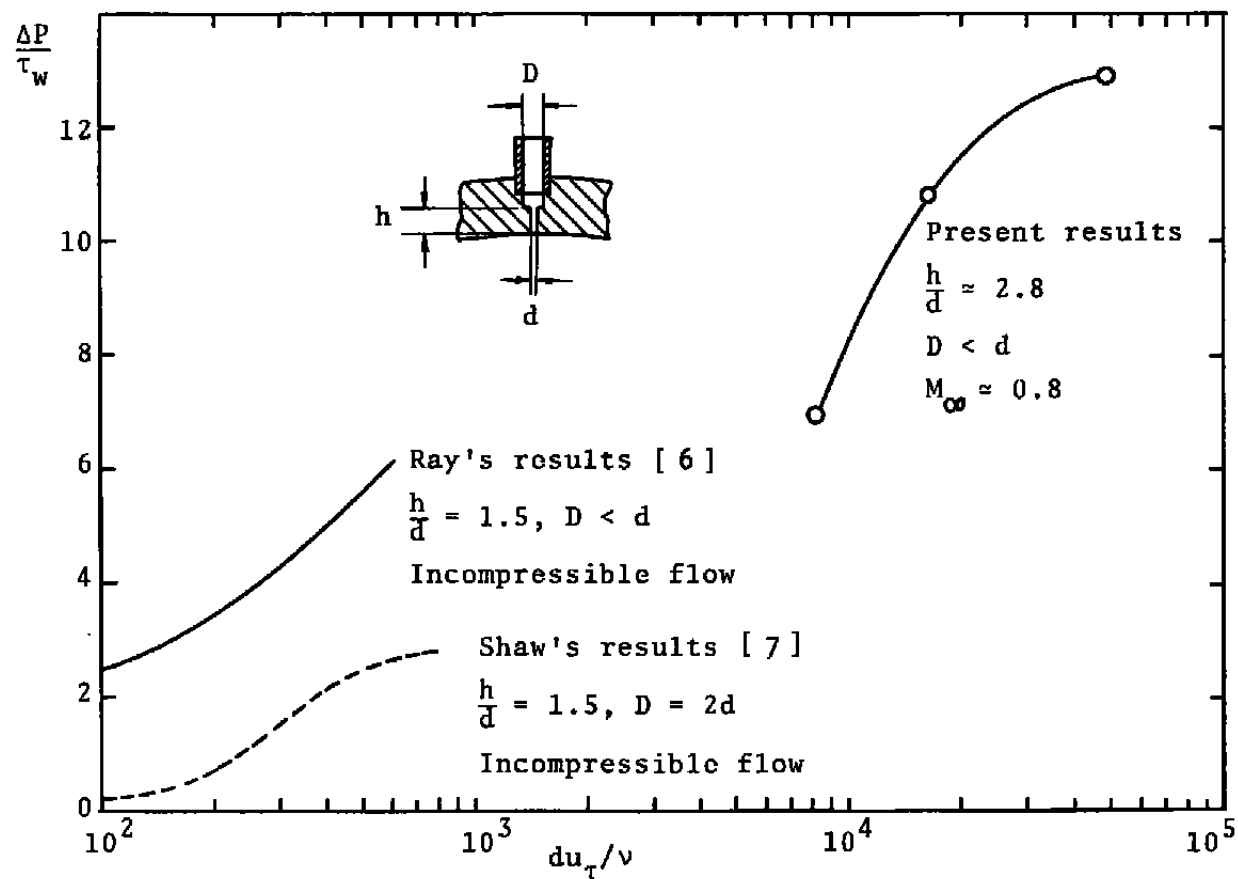


Figure 16. Dimensionless pressure error against Reynolds number.

number, $d u_T / v$. It should also be remembered that there is not a direct measurement of the mean orifice pressure in the present study since this was estimated from the pressure distribution over the major part of the orifice floor. This problem is more severe for the smallest diameter orifice since then the pressure taps did not cover such a large fraction of the orifice floor.

IV. THE MULTIPLE ORIFICE STUDY

The basic geometry of the multiple hole model was shown in Figure 4 and the model was mounted in the tunnel in a similar fashion to that suggested by the single orifice model mounting in Figure 3. Due to the location of the mounting bolts it was possible to rotate the model to yield a variety of test configurations. These configurations are indicated on Figure 17 along with the identifying notation. The individual holes were 0.5 inch in diameter and spaced 1.5 inches between centers. The hole depth was fixed at a value of 1.38 inches so that the ratio $h/d = 2.76$ was identical to that of one of the single orifice models tested.

Again the basic interest in the test lies in any measurement error incurred and in the distortion to the boundary layer downstream of the orifice location. From the studies of the single orifice model, it can be anticipated that the downstream effect for the 0.5 inch diameter model would not be too large (compared to the effect of the 3.0 inch diameter orifice).

Figure 18 shows the distribution of static pressure across the floor of the orifice for three representative configurations. It is seen immediately that the interference between adjacent orifices has the effect of increasing the pressure level in both orifices if the interacting holes are either in line or side by side. When the holes are aligned at 45° relative to the free stream then the pressure level is reduced in both

● closed
○ open

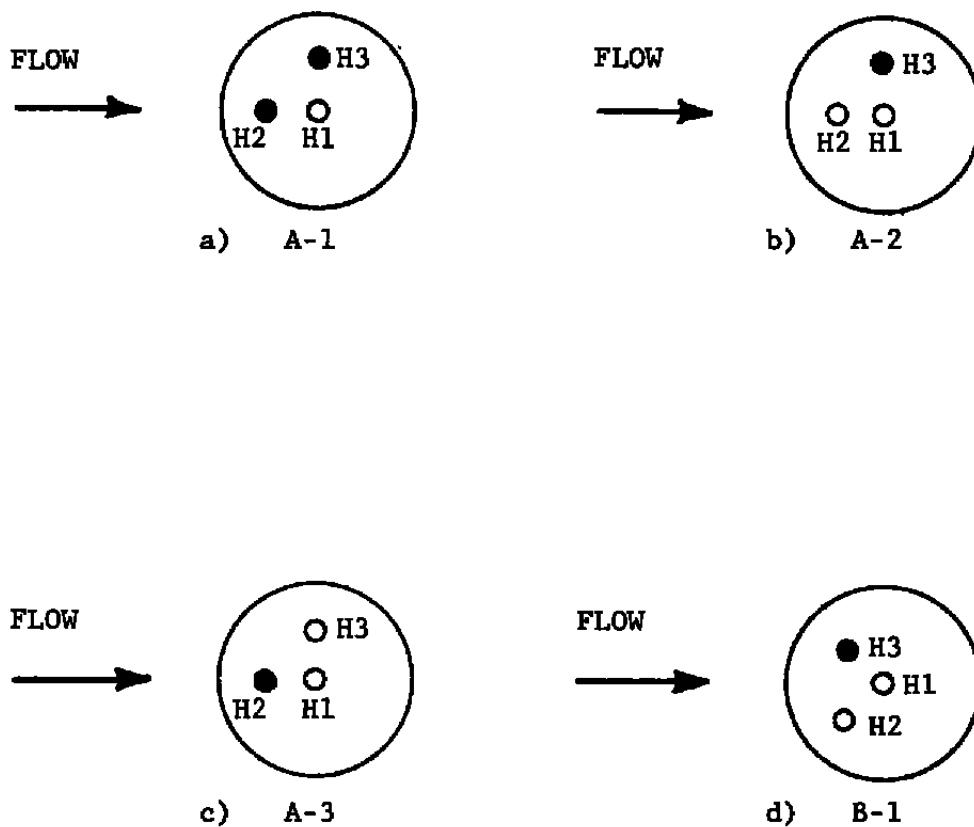


Figure 17. Hole Configurations for Various Multi-Hole Tests. The hole H1 is at the center of the block and is located at the 40" station on the tunnel center line.

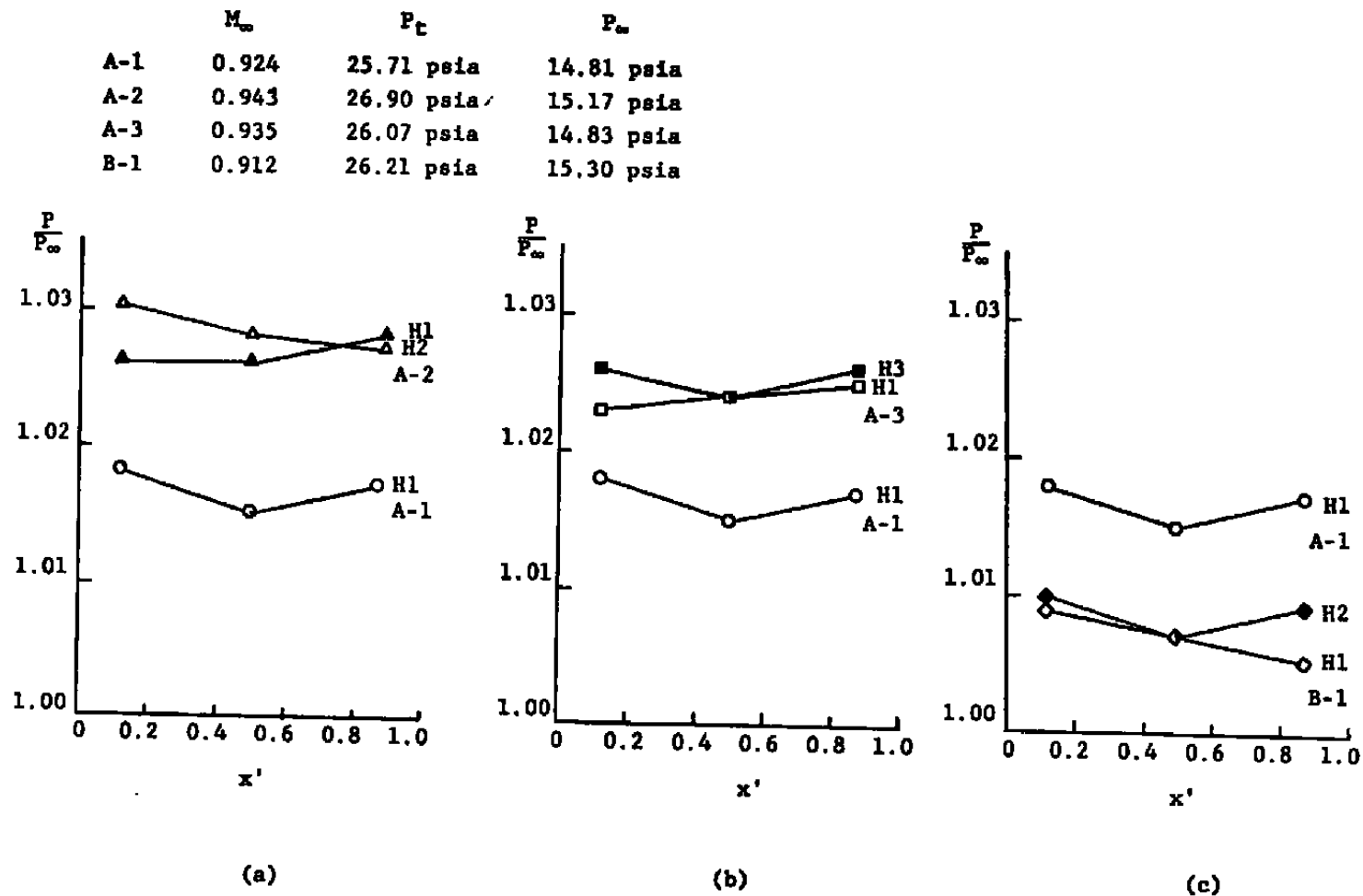


Figure 18. Pressure Distribution on Orifice Floor for Different Multi-Hole Configurations.

orifices and the recorded pressure would be nearer to the correct pressure (within the confines of $h/d = 2.76$ --see Figure 15). This result needs some explanation.

The flow into the hole is the primary reason for the over pressure recorded on the orifice floor⁽⁸⁾ and this mechanism would operate on each of the orifices independently. The only difference would be the local flow properties at the entrance of the individual holes and in this connection one feature of the pressure field established by a single hole is of importance. Ahead of the hole there is a general tendency for the pressure level to be higher than the free stream value and this is also true on the streamlines that pass by either side of the hole (Figure 19). It can be anticipated therefore that the pressure error for two holes side by side would be increased. At the same time, the pressure downstream of a single hole increases rapidly after the initial low pressure at the downstream lip of the orifice. Figure 11 indicates that the pressure has returned to the free-stream level within two hole diameters of the orifice. Hence it can be expected that the mutual interference would again result in an increase in indicated pressure level when two orifices are located directly along the stream. In this case the upstream hole should register the higher pressure level. The results of Figure (18a,b) support these suggestions.

When the two holes are not directly in line (configuration B1) then the situation is different. Downstream and to the side

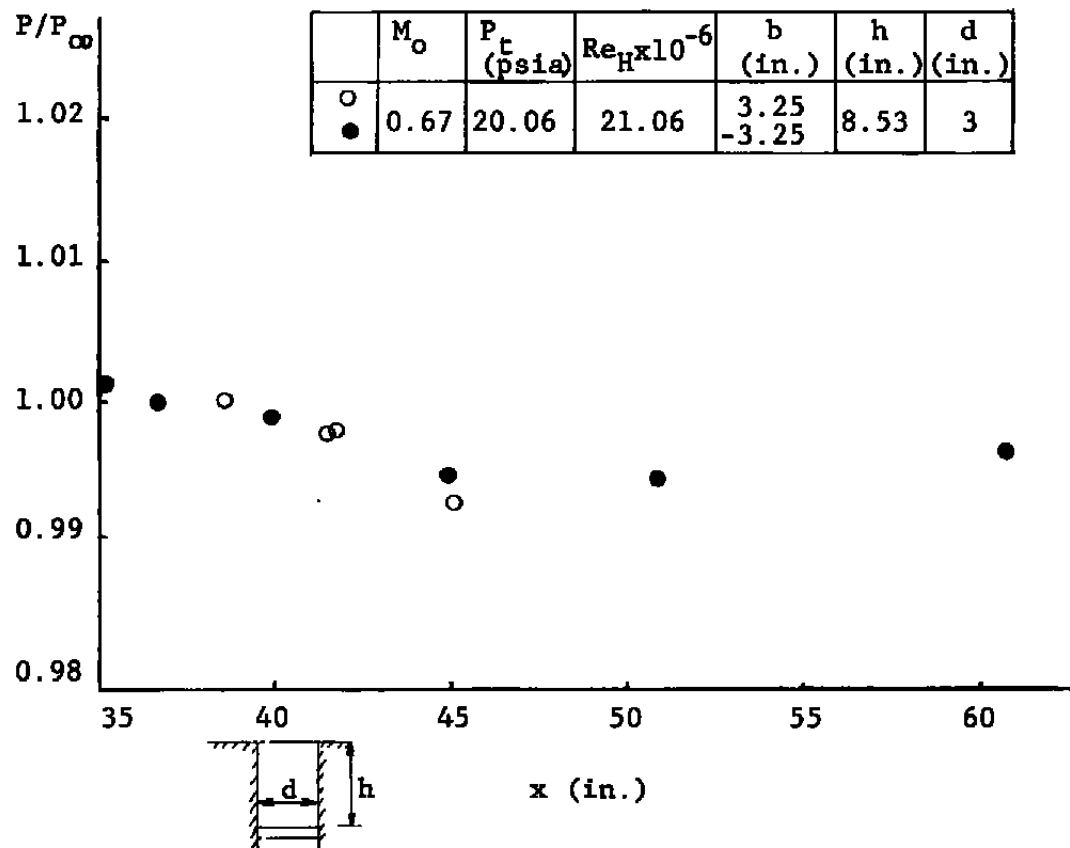


Figure 19. Static pressure distributions along the $b = \pm 3.25$ -inch lines.

of a single orifice (Figure 19) there is a large area of lower pressure which would lead to the expectation of a reduced pressure at the downstream hole. This is found in Figure (18c) but it is also found that the upstream orifice pressure level is reduced by a slightly smaller amount. It is not so obvious that this should be the case.

The ratio of hole diameter to hole separation distance was not varied in the present study. It could be anticipated that if the separation distance was increased then the possible beneficial interaction, as far as measurement error is concerned, may be lost. The existence of this favorable interference, if substantiated by subsequent testing, may be of some interest in model design.

Boundary layer traverses on the center line downstream of the multiple-orifice model were also measured. Figure (20) shows typical velocity profiles at the $x = 42.8$ inch location for the A1, A2 and A3 configurations. Here, there is no large change in the velocity profile and no obvious trend in the data as the hole interference is changed. This result is not too surprising in view of the fact that each orifice is only 0.5 inches in diameter (so $d/\delta \sim 0.7$) since, as indicated in Figure (21) for a single orifice, the profile distortion is a strong function of the ratio of hole diameter to approach boundary layer thickness. No velocity profiles were measured off the centerline for the multi-hole model.

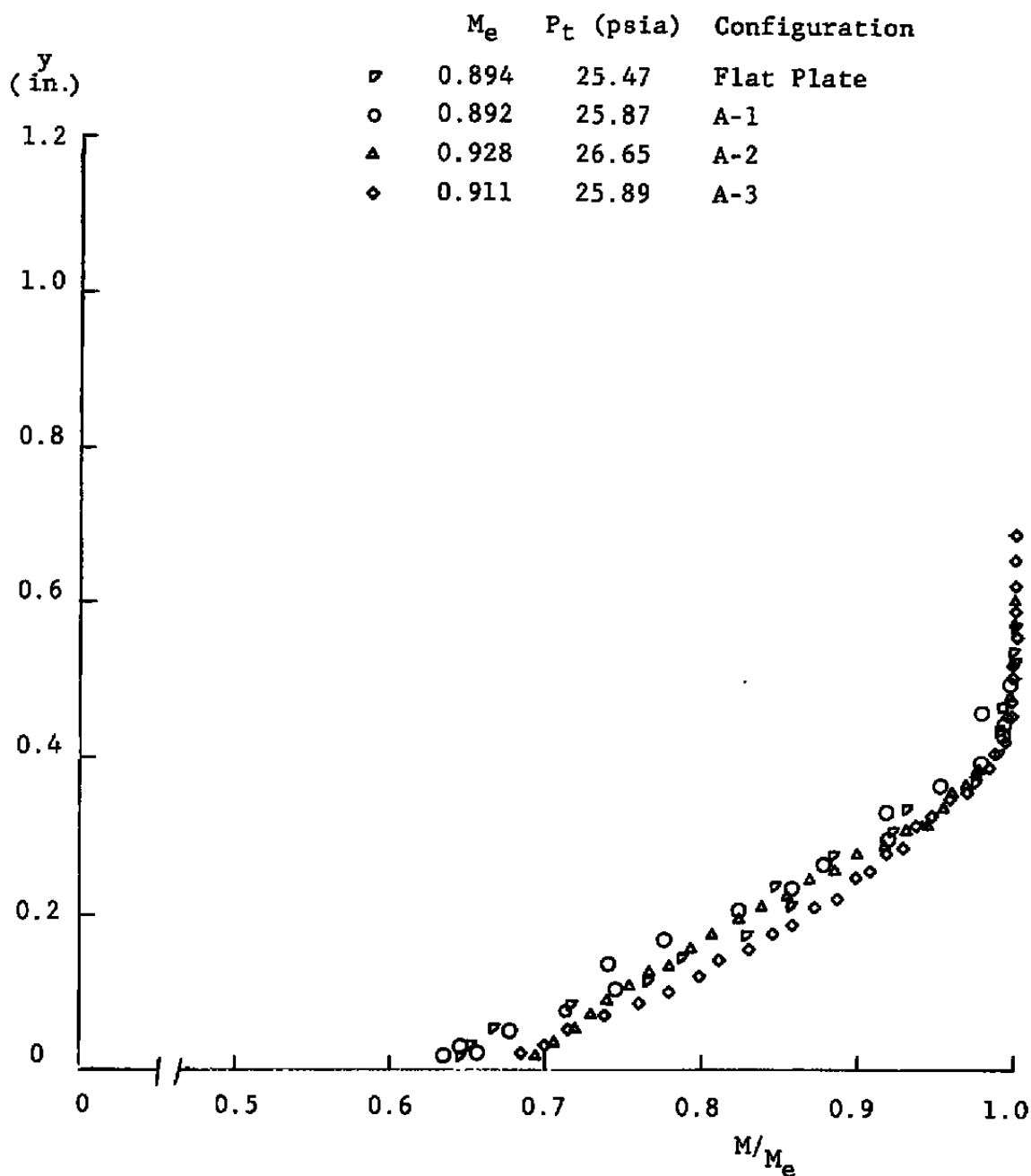
$x = 42.8''$


Figure 20a. Velocity Profiles, at $x = 42.8''$, Behind Various Multi-Orifice Configurations.

$x = 49.5''$

	M_e	P_t (psia)	Configuration
--	-------	--------------	---------------

○	0.905	26.33	Flat Plate
---	-------	-------	------------

□	0.905	26.10	B-1
---	-------	-------	-----

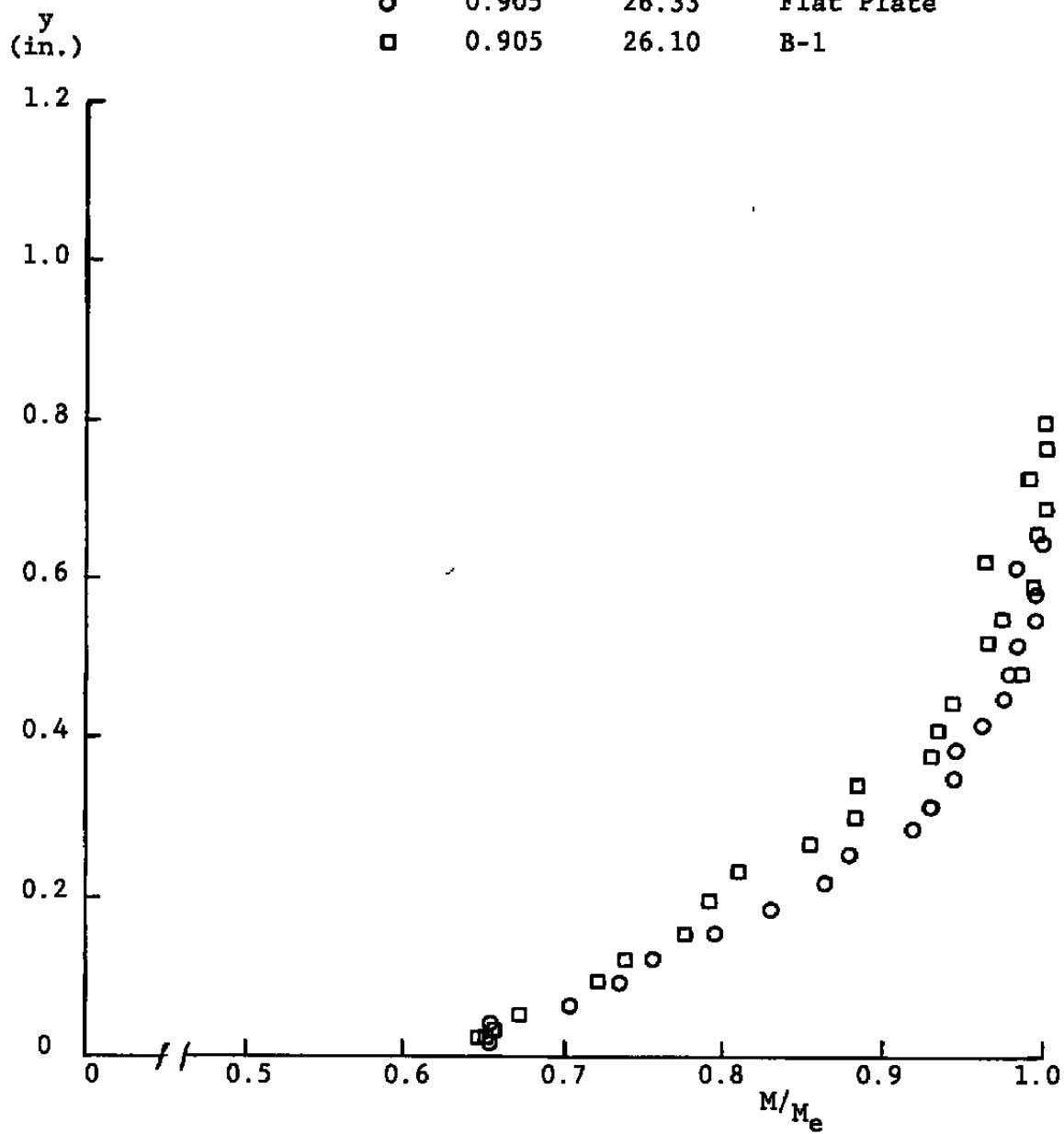


Figure 20b. Continued...

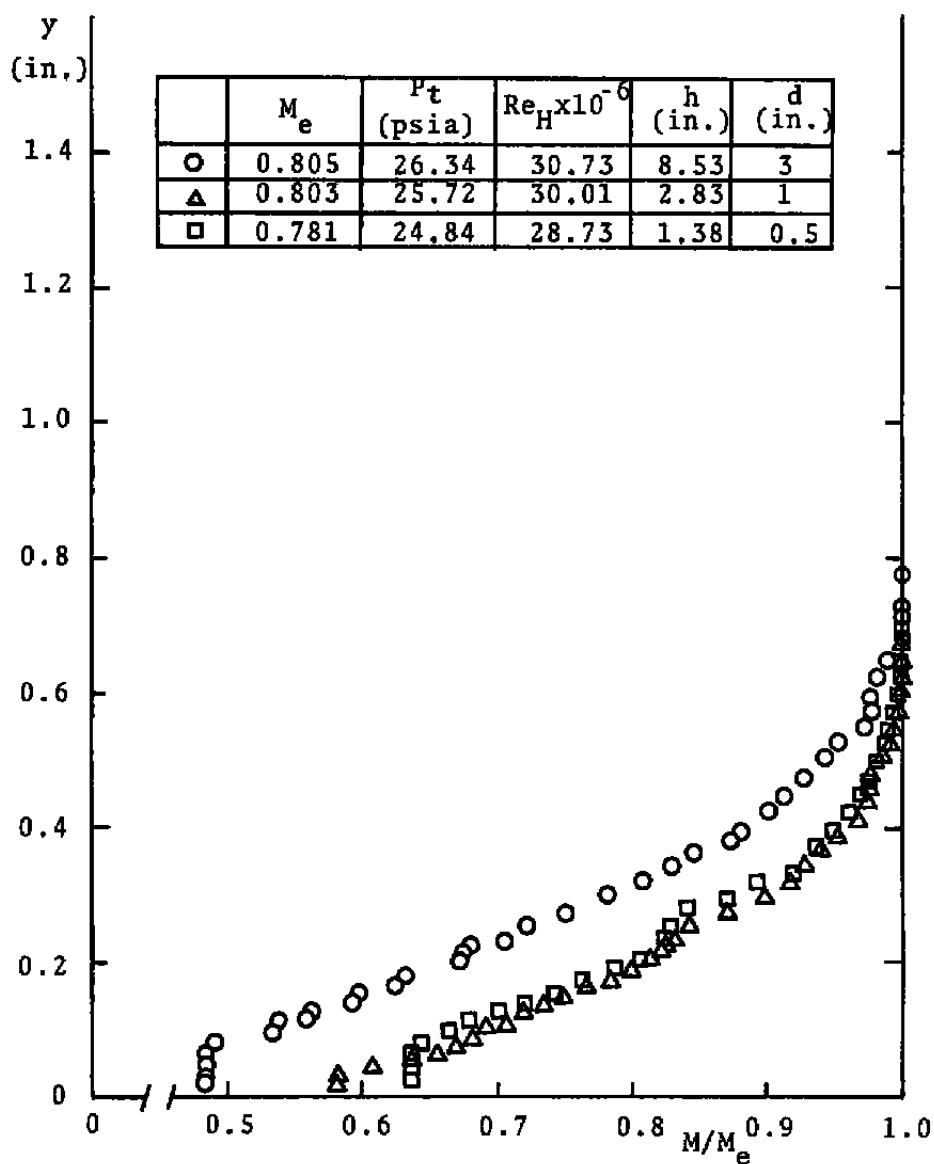


Figure 21, Velocity profiles at $x = 42.8$ inches with $h/d \approx 2.8$. Single Orifice Study.

V. SOME ANALYSIS OF THE DOWNSTREAM BOUNDARY LAYER

One of the interesting features of the external flow is the extent of the disturbance created in the boundary layer downstream of the orifice. In the present study it is only the mean flow quantities that can be discussed since no attempt was made to investigate the turbulence structure (other than the wall static pressure fluctuations). It is known, however⁽⁹⁾, that the turbulence structure will take a considerably longer time to return to equilibrium than does the mean velocity profile and any discussion based upon mean quantities alone will only give a lower bound to the extent of the disturbance.

The data from Figure (10) is replotted on Figure (22a) to give the spatial locus of the mean flow disturbance. From this figure it can be anticipated that the main distortion within the mean velocity profile will not pass out from the edge of the shear layer for a considerable downstream length from the disturbance. It is interesting to note that Kovosznay⁽¹⁰⁾ showed the strongest correlation between wall events and super-layer events occurred after a large downstream distance. It is of interest therefore to compare the rate of dispersion of the disturbance into the flow (Figure 22a) with the turbulent burst trajectories measured by Kline⁽¹¹⁾ at the edge of the viscous sublayer and these are plotted on Figure 22b. Some comments are in order.

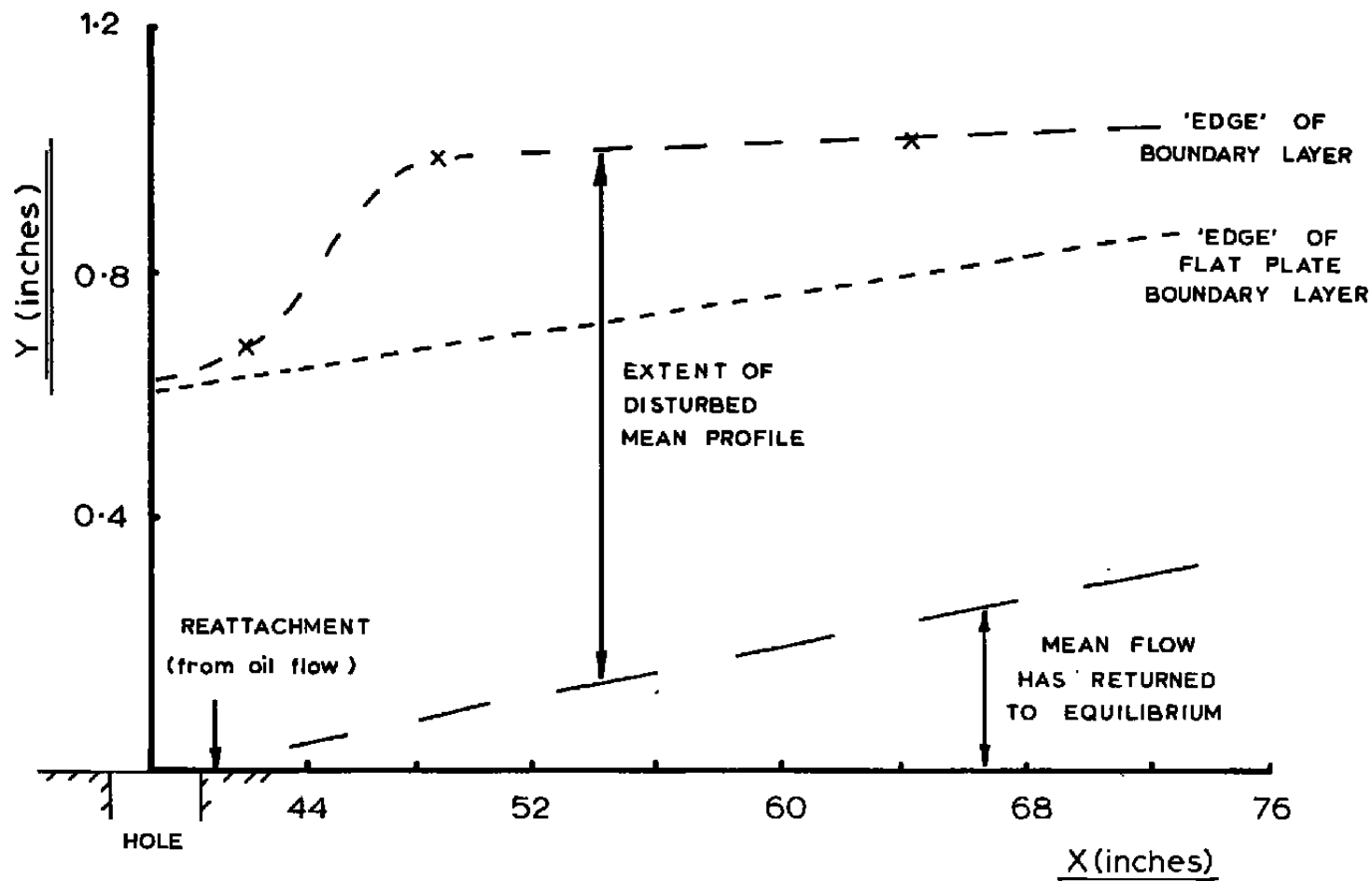


Figure 22a. The Disturbed Mean Velocity Profile.

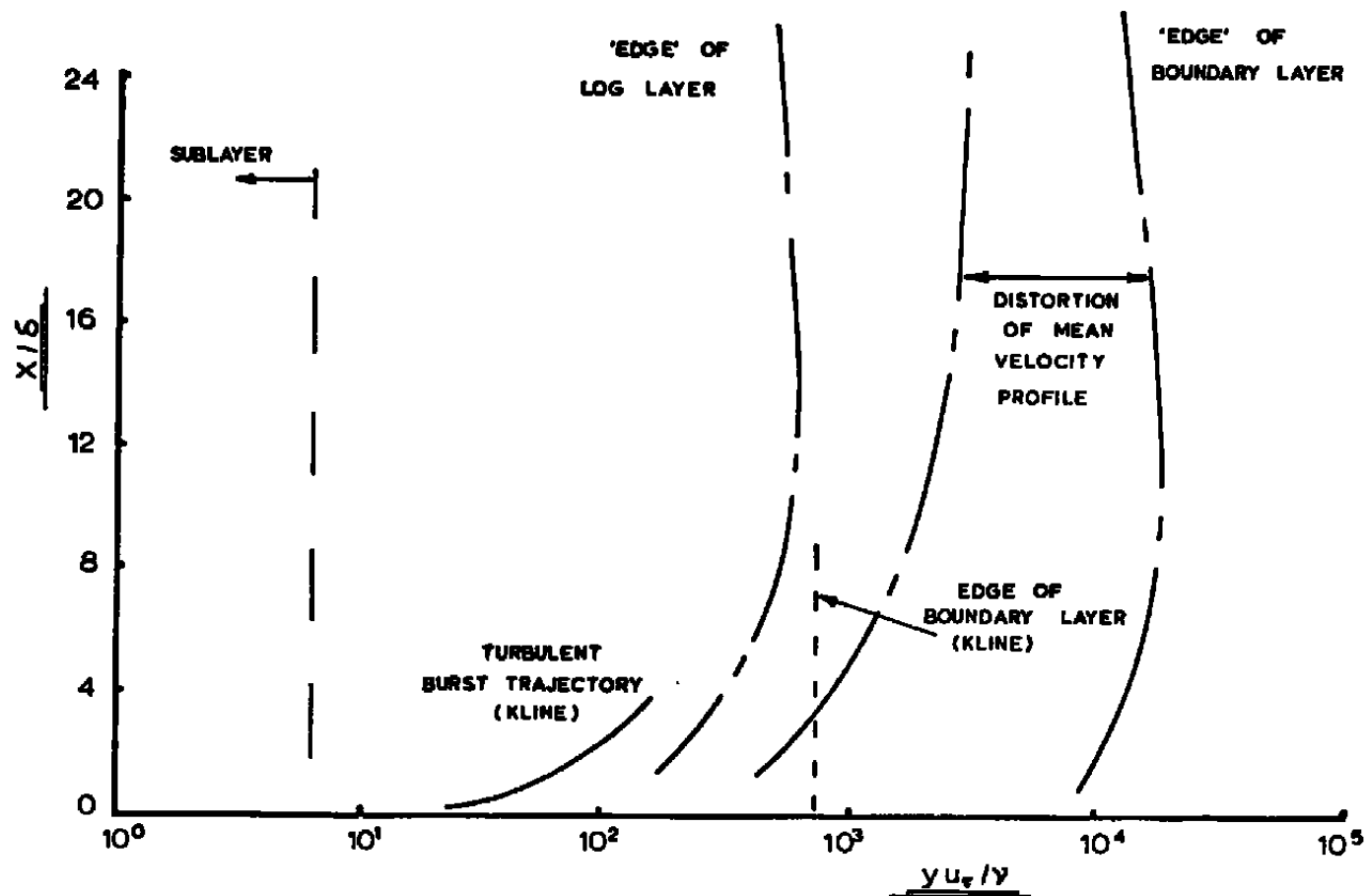


Figure 22b. The Distorted Mean Velocity Profile in Law of the Wall Coordinates.

The burst trajectories reported in Reference 11 were restricted to that region of the boundary layer for which $10 < y u_{\tau}/\nu < 120$ after which the individual events become indistinguishable from the general wake-region turbulence. On the other hand, velocity profiles sufficiently close behind the hole were not recorded, in the present study, for the propagation of the disturbance in the region $y u_{\tau}/\nu < 300$ to be determined. The scale $y u_{\tau}/\nu$ depends heavily upon the value of u_{τ} which must be obtained from a curve fit of the measured velocity profile in the present work. It is well understood⁽¹²⁾ that the level of free-stream turbulence can have a large effect on the skin friction of a turbulent boundary layer. This fact could be responsible for the apparently rather high value of $\delta u_{\tau}/\nu$ recorded in the present work. It is unlikely that the modest effects of compressibility would increase this factor by an order of magnitude over the incompressible flow flat plate values. Figure (23) shows typical velocity profiles plotted in the inner variables where it is seen that $\delta u_{\tau}/\nu > 10^4$. For these reasons it is probably not too meaningful to make further comments concerning the curves in Figure (22b).

Some indication of the nature of the flow into a large hole is shown by the oil flow photograph of Figure (24) and the sketch of the basic flow features in Figure (25). Most prominent is the region of high shear just downstream of the hole and also the flow into the hole. The flow approaching the downstream lip of the orifice will be inclined somewhat into the hole and

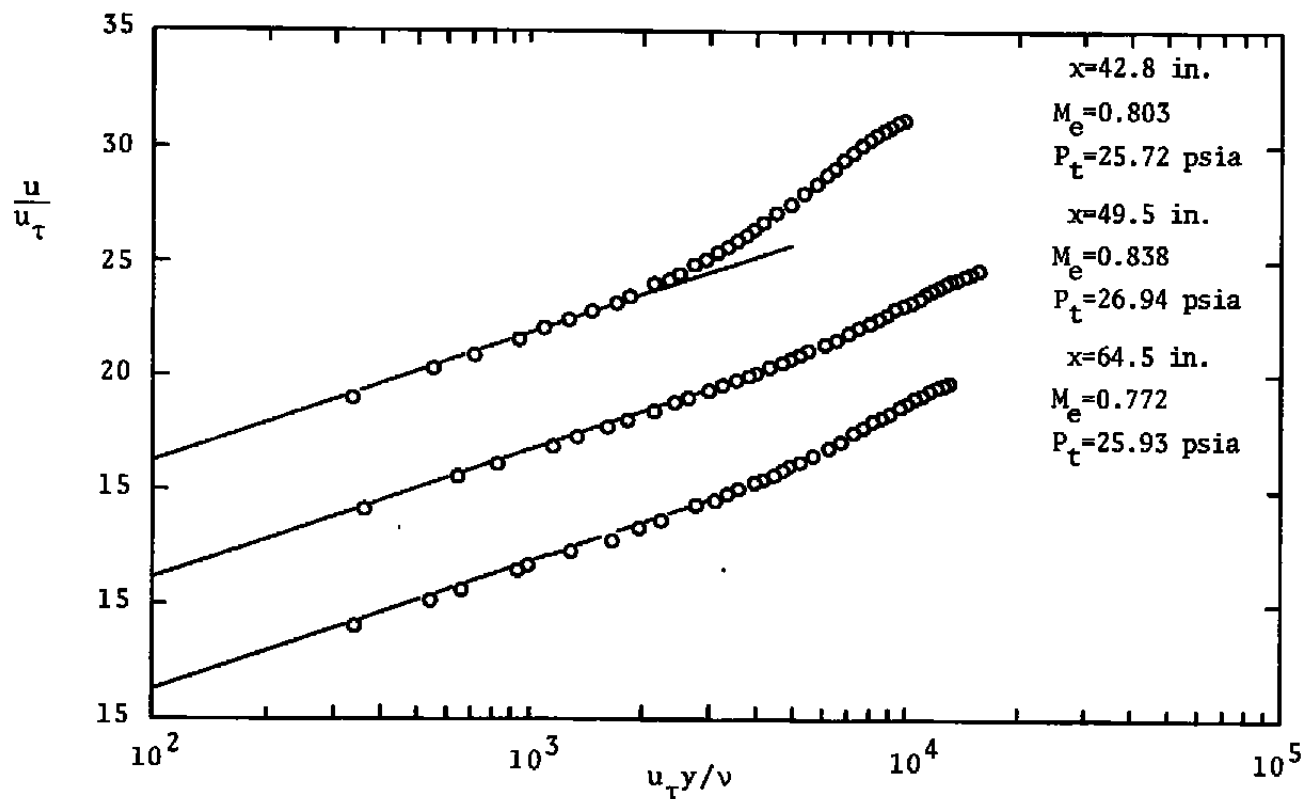


Figure 23a. Mean velocity profiles at three different locations with $d = 1$ inch and $h = 2.83$ inches.

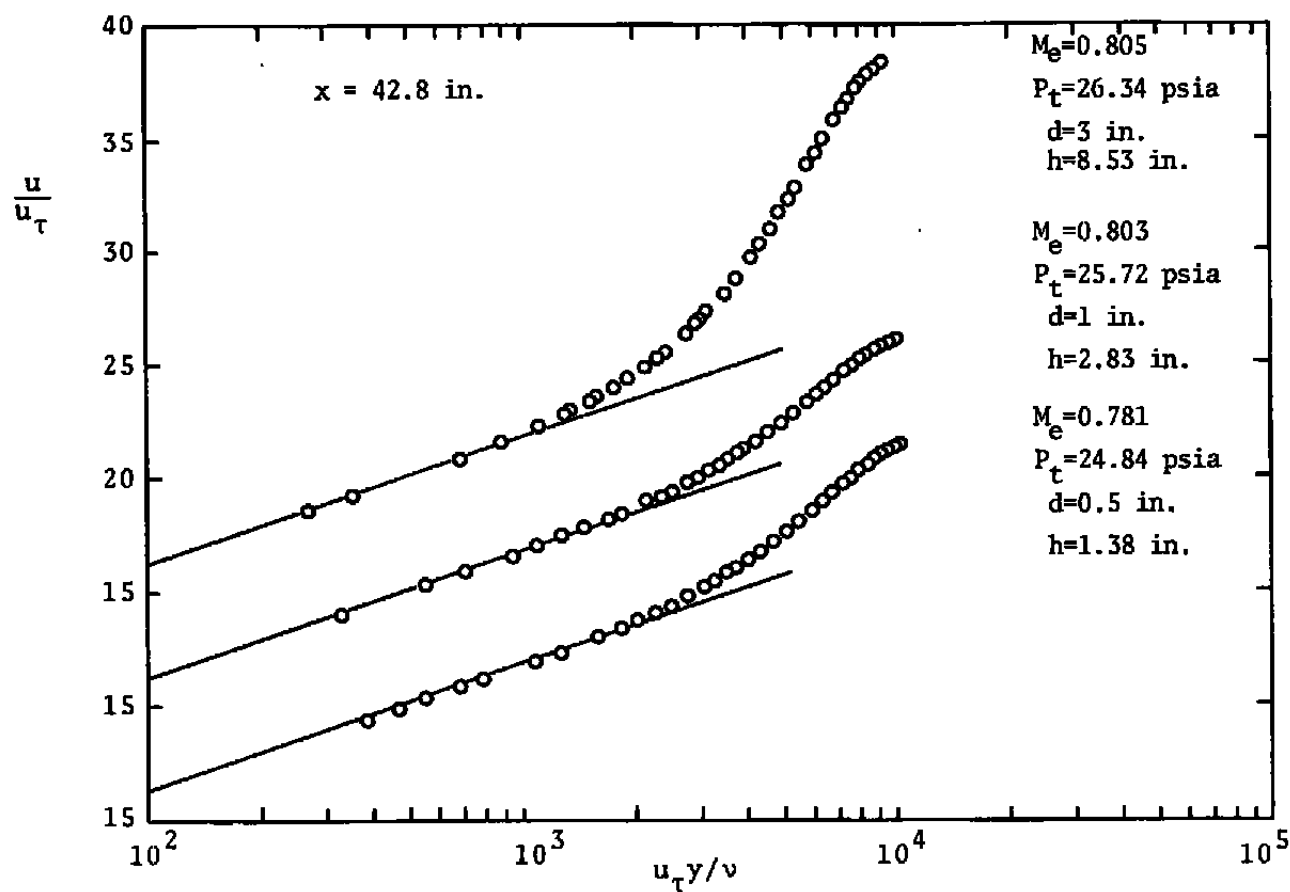


Figure 23b. Mean velocity profiles at $x = 42.8$ inches with nearly constant h/d ratio (≈ 2.8).

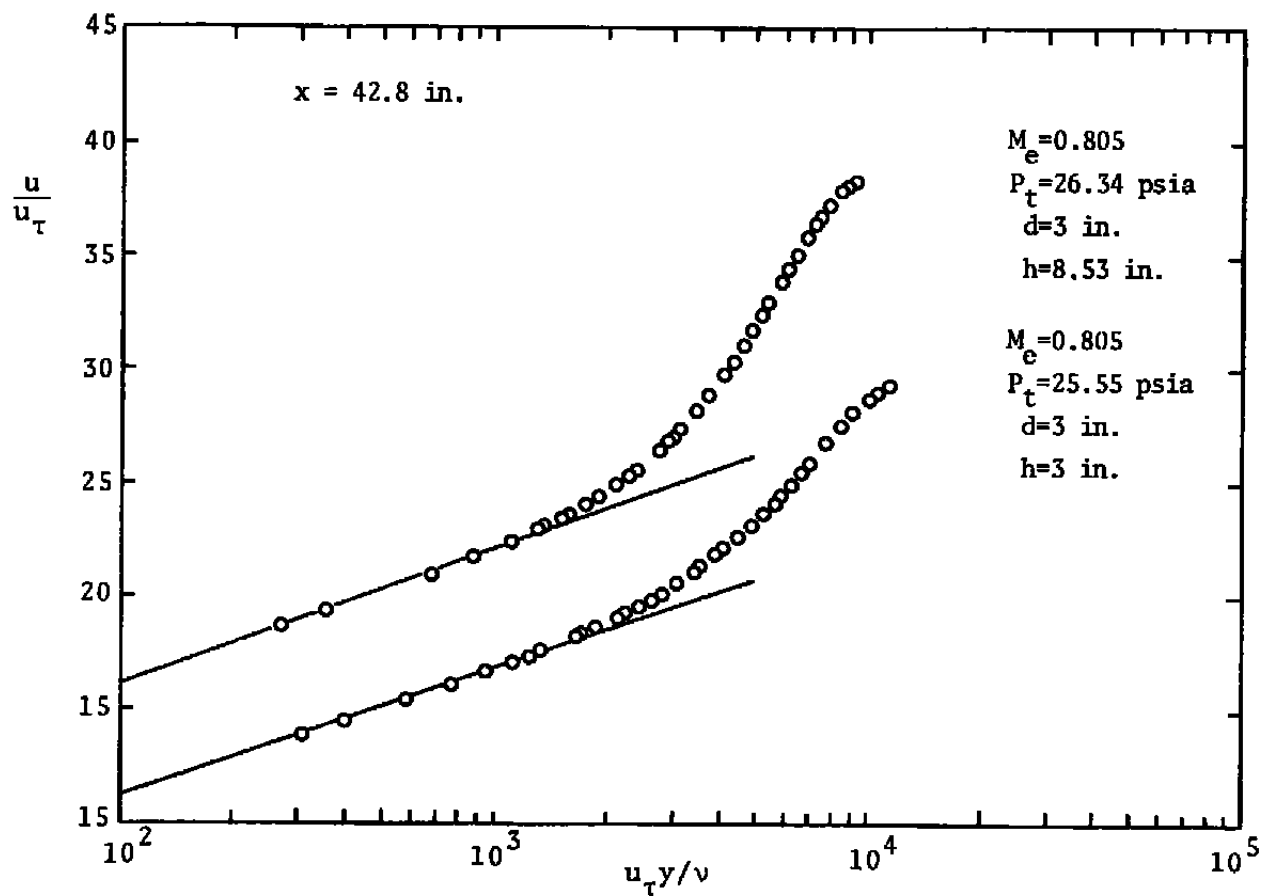


Figure 23c. Mean velocity profiles at $x = 42.8$ inches with different hole depths of 3-inch hole diameter.

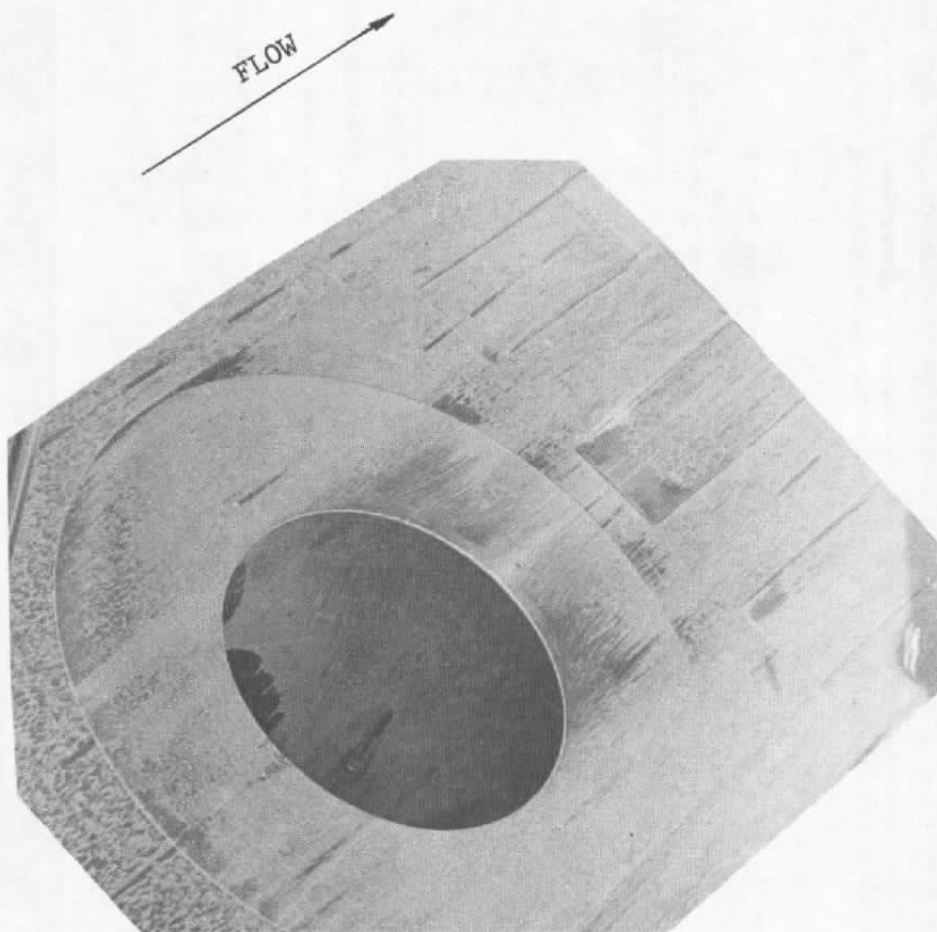


Figure 24. Oil Flow Pattern for the Three-Inch Orifice.
Flow towards the top right-hand corner.

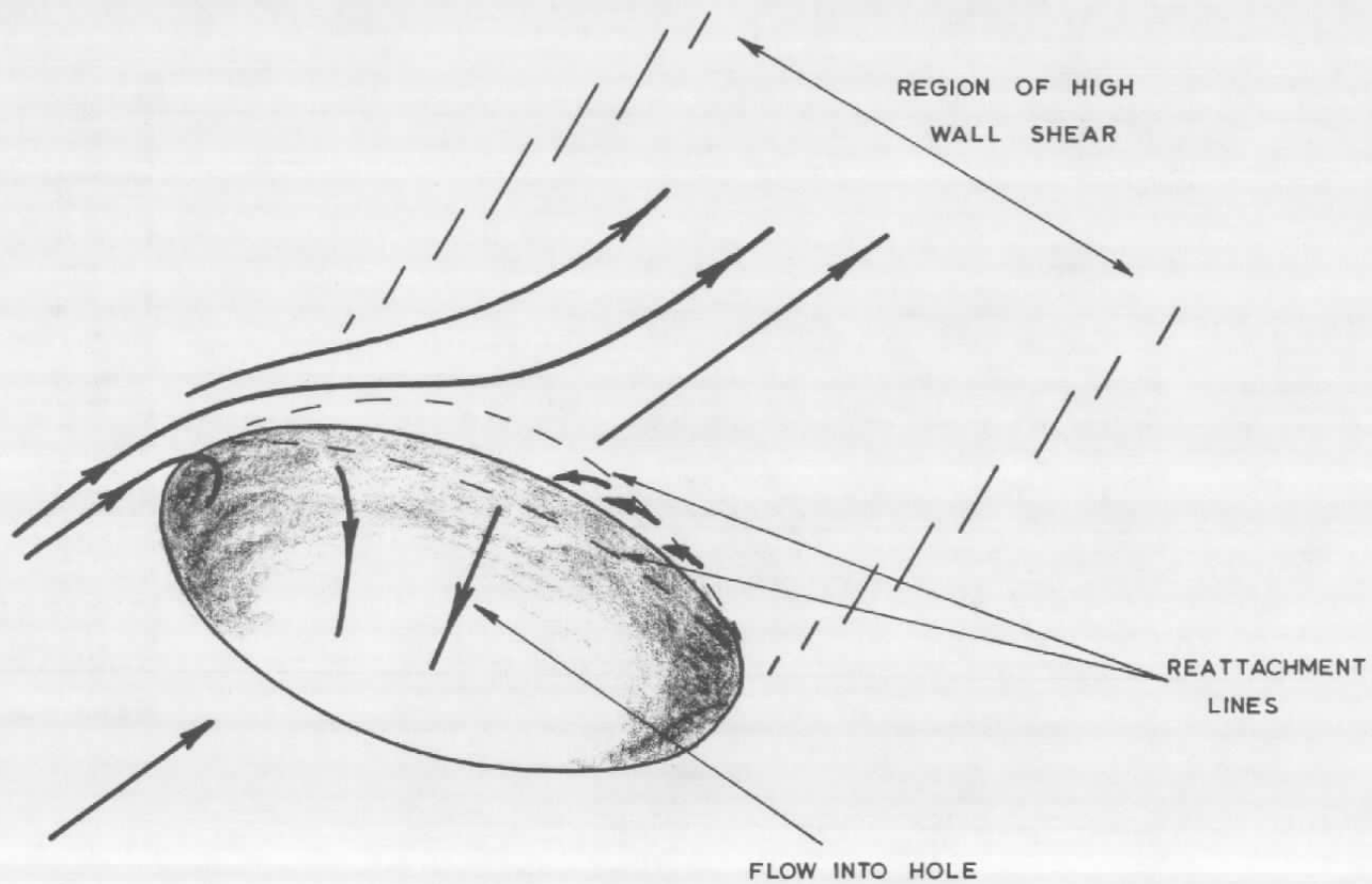


Figure 25. Diagram of Flow Taken from the Photograph of Figure 24.

cause a reattachment to occur on both the orifice wall and the surface downstream of the hole. The flow into the hole is quite well developed but, due to the dictates of continuity, cannot be simply inflow. It is not possible to determine, from the oil flow study, any unsteadiness that may be present in the flow. The schlieren photograph of the flow over the hole (Fig. 26) does indicate some weak wave motion but nothing as pronounced as that noted in the two-dimensional cut-out tests of Krishnamurty⁽¹³⁾ -- the work of Wieghardt⁽⁵⁾ would indicate, however, the presence of considerable unsteadiness under some geometry conditions.

At the sides of the hole there is a clear inflow into the orifice but it is not clear if a trailing vortex system is established or not.

To determine the seriousness of unsteady effects (acoustic waves) created in the hole on the boundary layer downstream of the hole, steady state computations were made. First, results from a computer program established at ARO, Inc. (by J. C. Chien of ETF) were obtained. This program calculated the laminar incompressible flow over a two-dimensional cavity and could, therefore, only be considered to be a very qualitative indication of the actual orifice behavior. Also, no check was made on the effect of the very short inflow and outflow sections used in the program. In order to more closely simulate the turbulent mixing of outer and cavity flow, the viscosity was set to $\nu = 0.001$ (0.0002 would be the molecular viscosity). Four cases were computed, $\delta_1/d = 0.33$ and $h/d = 3$ and 1, and $\delta_1/d = 0.66$, and $h/d = 3$ and 1. Here δ_1

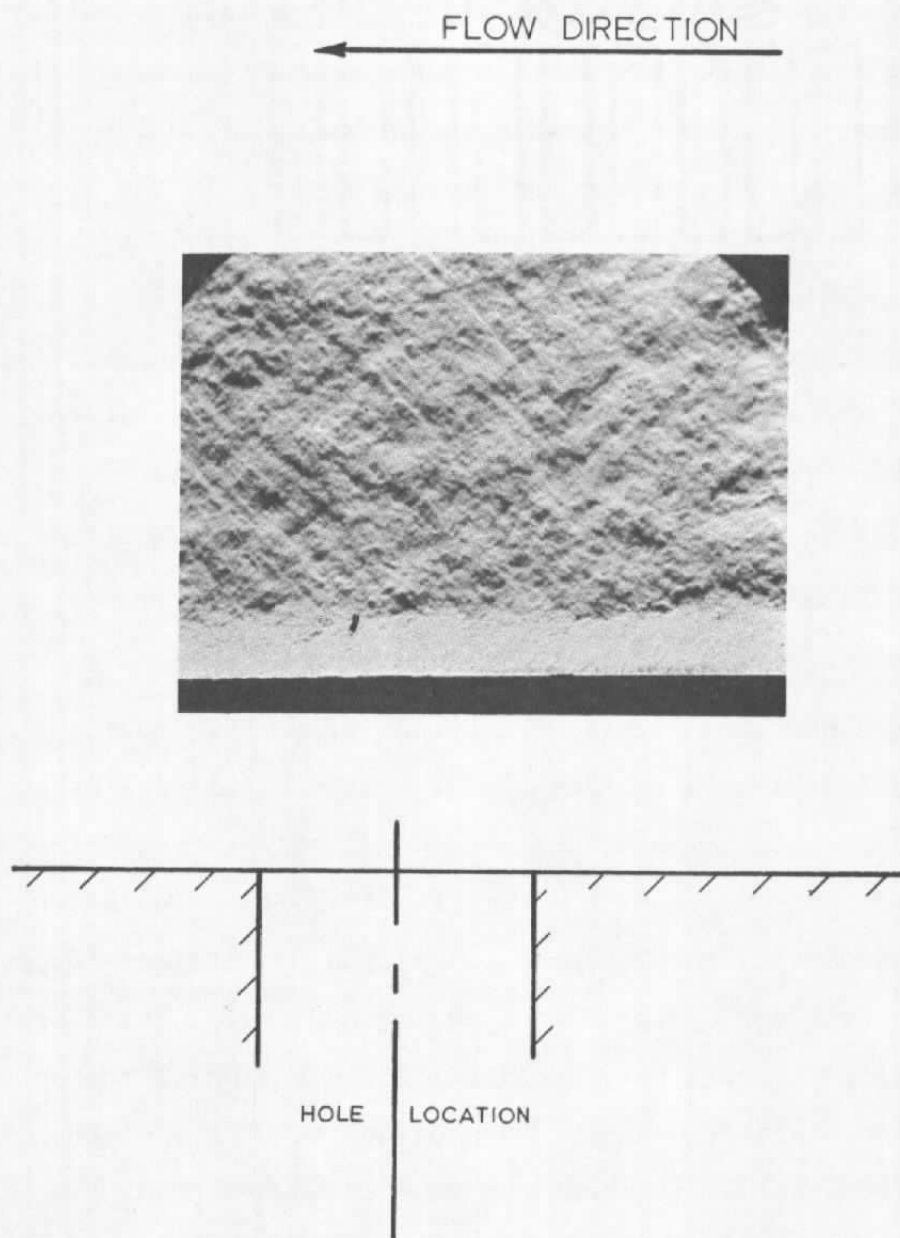


Figure 26. Typical Schlieren Photograph of Flow Over 3-Inch Diameter Hole with $h/d = 2.84$.

is the initial boundary layer thickness, d and h the cavity width and depth. The important finding was that the boundary layer profile downstream of the cavity was within the computation accuracy, equal for the two d/h cases considered. Otherwise, a less full profile was observed downstream of the cavity than that of the profile upstream and exhibits the basically expected more "wake"-like profile behind the cavity disturbance. The fact that the deep and shallow cavities produced completely identical profiles is, however, in disagreement with the test results, which show consistently a strong dependence of depth in the sense that a deeper hole affects the downstream profile more than a shallow hole.

Further calculations were carried out with a program for turbulent, incompressible flow developed by Bitte⁽¹⁴⁾. For the inlet profile, a logarithmic (turbulent) profile was chosen for an effective boundary layer thickness equal to the cavity width d . To establish a relation to the ARO program, the first computations were also made for a constant $\nu = 0.001$ as opposed to the varying eddy viscosity coefficient which the program can compute. Here, different values for the downstream profiles were obtained for the cases $h/d = 0.5, 1.0$ and 2.0 . However, the differences in these profiles (two hole diameters downstream of cavity trailing edge) were not indicating a marked increase of boundary layer disturbance with increasing h/d , although the slight change exhibited is in the sense of the experiments. The results are shown in Fig. 27. It can be concluded from

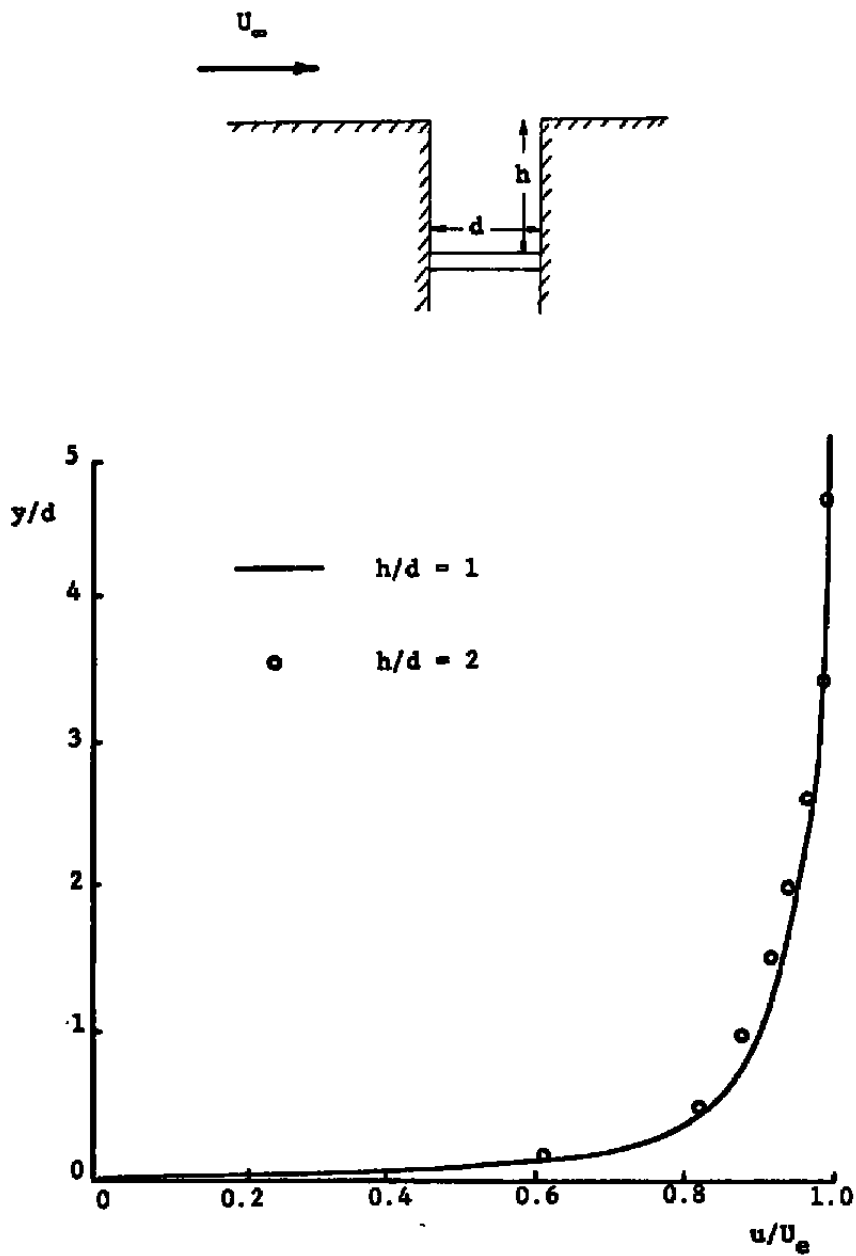


Figure 27. Calculated profiles at $x/d = 2.0$ downstream of hole.

these calculations that unsteady effects are very marked in the experimental data. The preliminary results make it very desirable, however, that the computations be continued to eliminate inaccuracies due to boundary conditions and to extend the computations to the variable turbulent viscosity in the flow field.

VI. WALL PRESSURE FLUCTUATIONS

It is important that some understanding of the turbulence structure downstream of the orifice be established. Ideally, this would be attempted via some non-intrusive measurement of the complete Reynolds stress tensor and of the correlation between pressure and velocity. Lack of instrumentation forbade such a program in the present work and only wall pressure fluctuation could be measured. In addition to this, the scope of the investigation was very limited with only the zero time delay two-point longitudinal correlation being determined. This measurement gives, via a 'correlation length', an indication of the scale of the turbulent motion. In simple physical terms we can consider this correlation length as the maximum spatial distance over which the events at one point influence conditions at another point in a statistical sense. Since such a study is not a central part of the present work it was not pursued in any detail. More information in connection with the instrumentation is given by Wu⁽¹⁵⁾.

Two 0.062 inch diameter PZT-5H piezoelectric elements were mounted in the tunnel as shown in Figure (28) and the data was collected via the instrumentation shown in Figure (29). The signal from the transducer was amplified by the Kistler charge amplifiers and then passed through a high-pass filter to remove the DC shift resulting from the temperature sensitivity of the PZT element. It should be noted that no attempt was made to acceleration compensate⁽¹⁶⁾ the transducer or to vibration

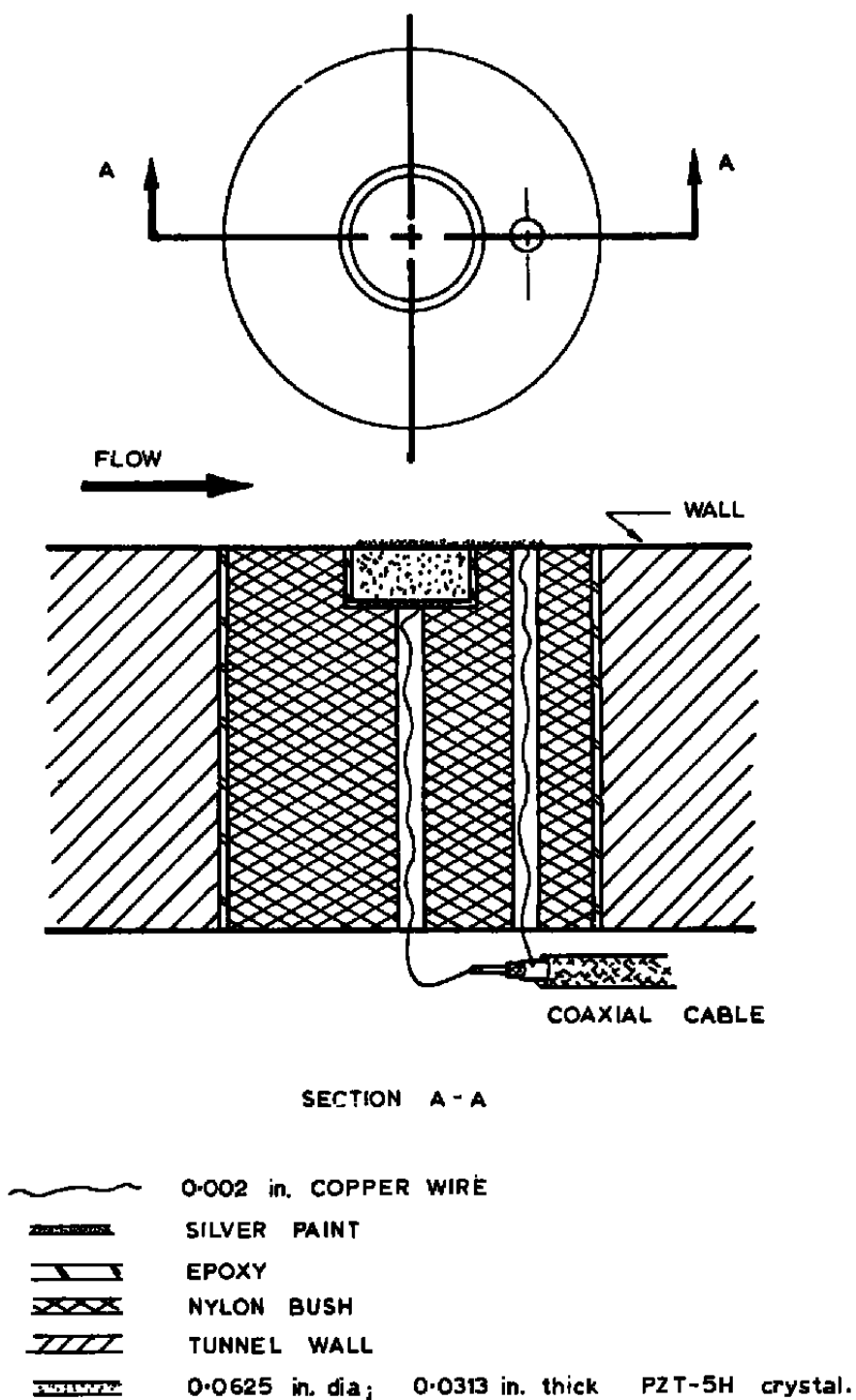


Figure 28. The Miniature Pressure Transducer.

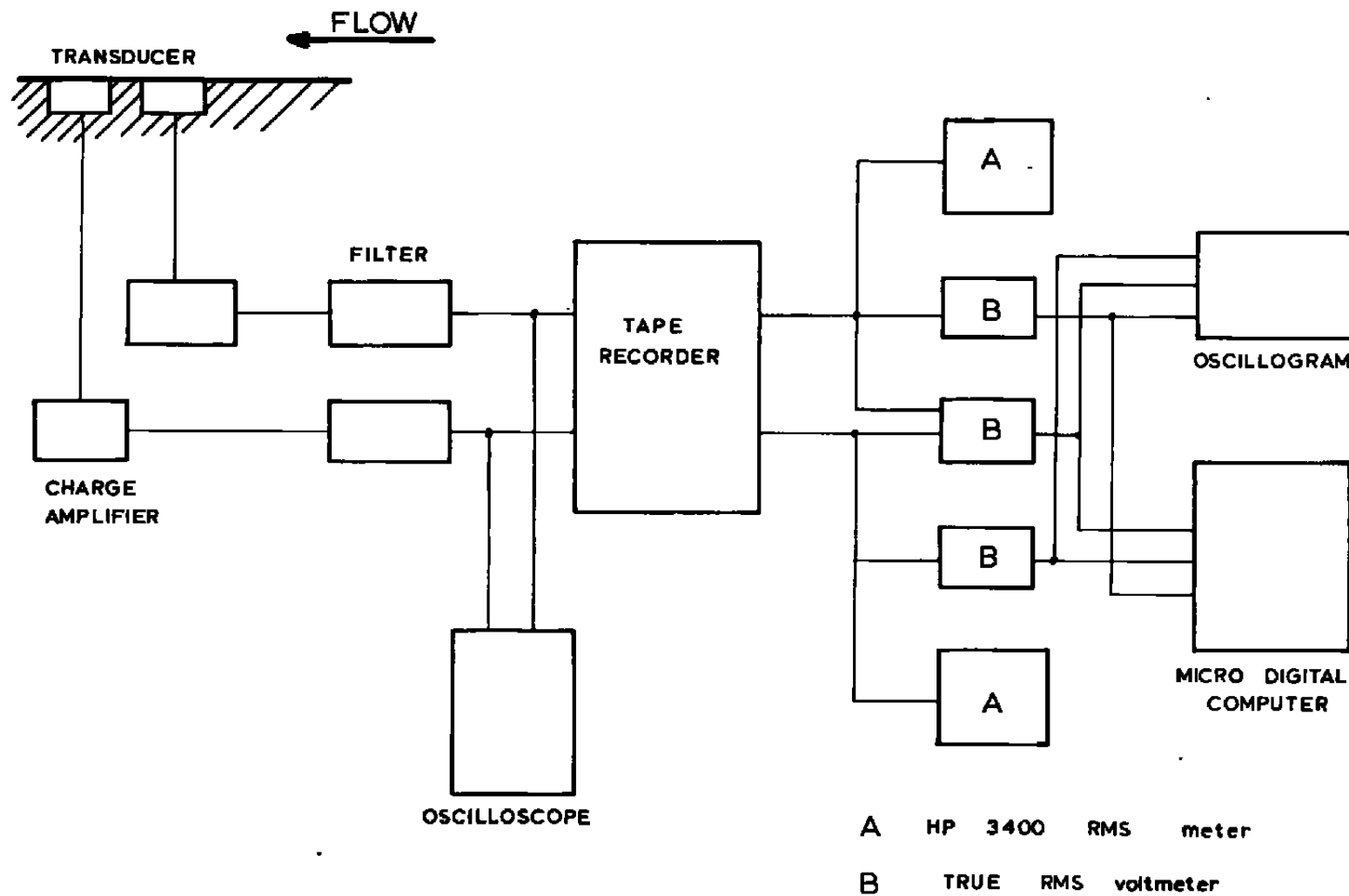


Figure 29. Block Diagram of Instrumentation.

isolate the mounting. Hence, the recorded signal from the transducer would be the sum of both the pressure fluctuations and the acceleration components. It can be anticipated however that the correlation length for the vibration mode would be great compared to the pressure fluctuation correlation length and hence the acceleration would largely result in an origin shift for the pressure correlation function.

Before presenting the results it is pertinent to make a comment about the transducer size in relation to the scale of the pressure field being measured. Willmarth⁽¹⁷⁾ shows the measured RMS wall pressure as a function of measuring area and this is replotted on Figure (30). The present data is recorded from an instrument with $u_\tau d/\nu \sim 600$ and hence is on the 'flat' part of the curve. The data shown by Willmarth for very small values of $u_\tau d/\nu$ were obtained from pinhole microphones whose cavity resonance frequency was of the order of 20 K Hz. No information is given about the frequency response of the RMS meter used to determine the RMS pressures from such microphone output, but if the cavity resonance frequency were included then a substantial error would be introduced and the large increase in RMS pressure explained at small $u_\tau d/\nu$. Bull⁽¹⁸⁾ has examined this problem and has indeed shown a significant modification to the spectrum at the higher frequencies when the pin-hole microphone is used. Willmarth explains the RMS pressure increase as being due to the very intense pressure pulses, as reported by Emmerling⁽¹⁹⁾, which occur at isolated points in the

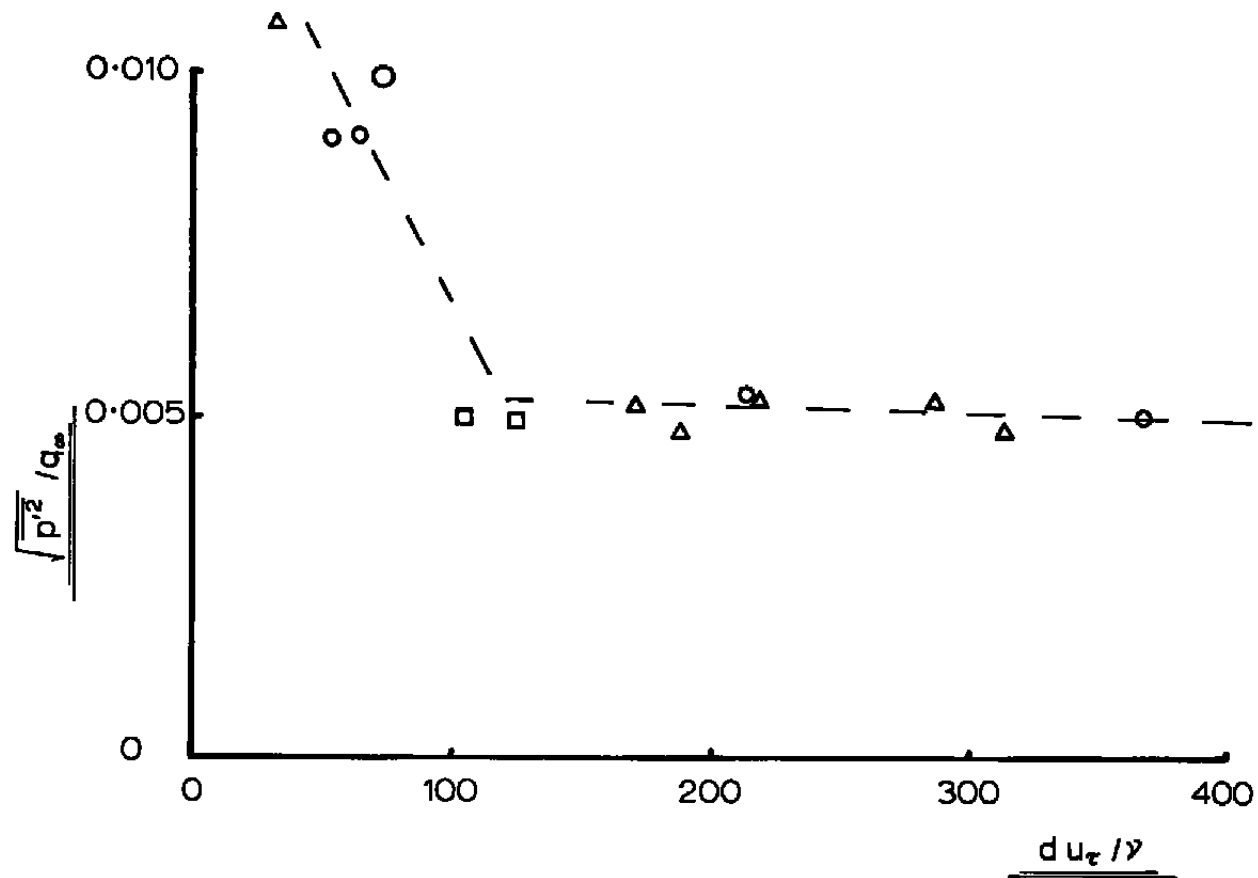


Figure 30. Variation of RMS Wall Pressure Fluctuation with Transducer Diameter. After Willmarth(17).

flow. This argument is not convincing since the RMS pressure must be a temporal average at the measurement point and, indeed, as the size of the measurement station is reduced, the probability of encountering an intense burst during a given sample is also reduced. It is unlikely that the effect is real as far as the determination of the RMS pressure is concerned. For a fine resolution of the structure in terms of a spatial correlation then the considerations would be somewhat different. It will be supposed in the present instance that the transducer size is adequate for the application in hand.

The zero time delay spatial correlation function, R , where

$$R = \frac{P'(x_1, y, t) P'(x_1 + m, y, t)}{\sqrt{P'^2(x_1, y, t)} \sqrt{P'^2(x_1 + m, y, t)}}$$

has been determined for both the flat plate flow and for the flow directly downstream of the three inch diameter orifice. This function defines the spatial region over which the local flow behavior, in a statistical sense, is influenced by the conditions at the control point at a given point in time. The zero time delay correlation function was determined from a true RMS meter circuit based upon an Analog Devices AD531K unit.

The results of the measurements are shown in Figures (31) and (32). It is clear that the spatial correlation function decreases with the separation distance between the two points as indeed it should.

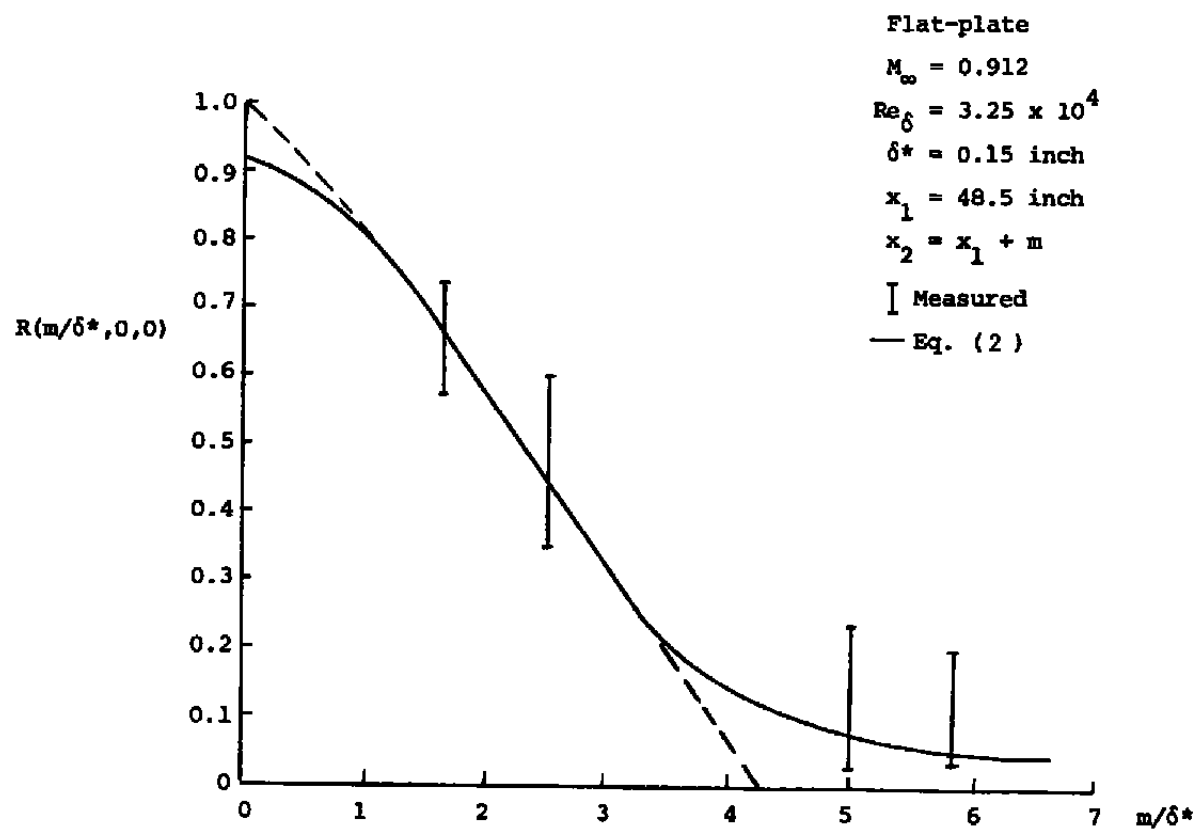


Figure 31. The correlation coefficient at the flat-plate.

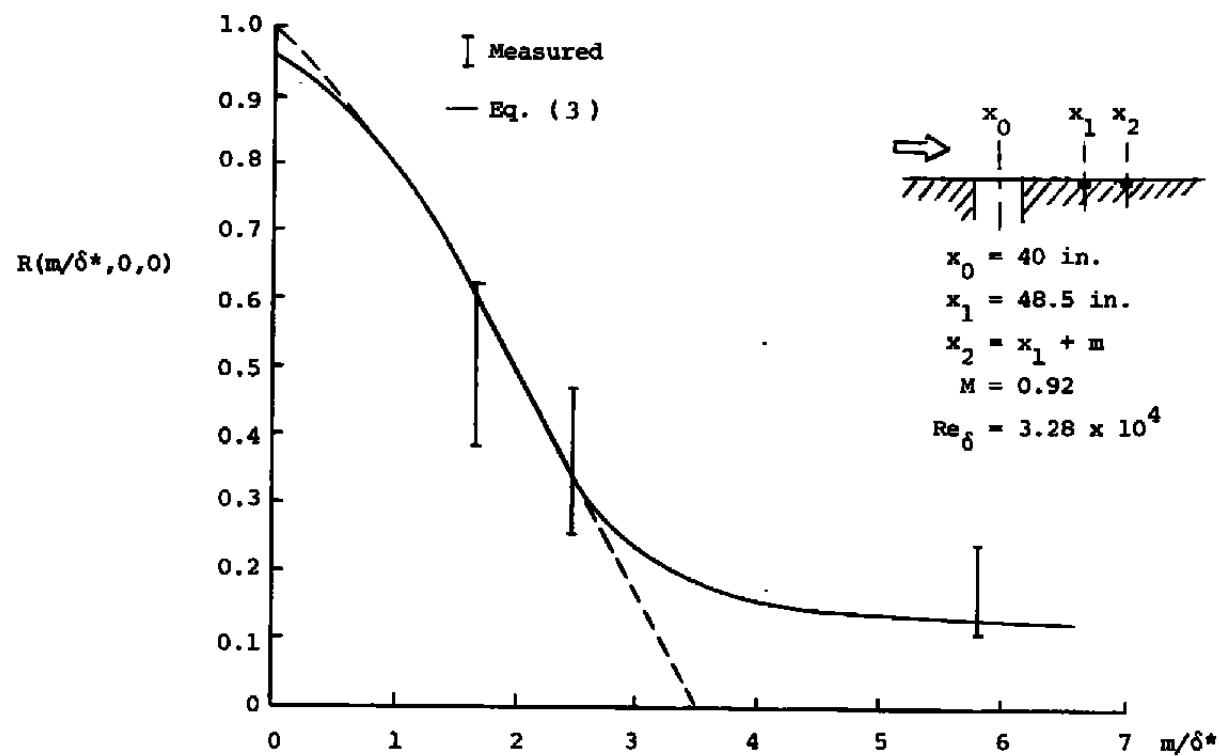


Figure 32. The correlation coefficient behind orifice.

The empirical representation which may be used as a basis for the calculation of structural response to turbulent boundary layer excitation and proposed for the spatial correlation function is

$$R = \sum_n A_n e^{-nk^2 m^2 / \delta^2} \quad (1)$$

This form for the spatial correlation function can be made to fit the experimental data as accurately as required but a two-term approximation is suggested herein for the spatial correlation. This becomes

$$R = 0.11 e^{-(m/1.2)^2} + 0.81 e^{-6(m/1.2)^2} \quad (2)$$

for the flat-plate flow and

$$R = 0.14 e^{-(m/1.2)^2} + 0.81 e^{-9(m/1.2)^2} \quad (3)$$

for the flow behind the orifice. These expressions are compared with experimental data in Figures (31) and (32). The dashed line towards $R(o,o,o) = 1.0$ is a theoretical result since the correlation function used is defined to pass through that point. However, from the curve fitting of the data points, the solid line passing $R(o,o,o) = 0.92$ is used for the minimum deviation of the data at larger spatial separation -- the region of greatest interest in the present study.

The lower dashed line is drawn to define the correlation length of the turbulence. This length is approximately $5/8$

inch and 1/2 inch for the flat-plate flow and behind the orifice, respectively. That is, the correlation length of the turbulence is longer on the flat-plate than it is behind the orifice which implies that the eddy size near the wall for the flat plate is larger than that near the wall behind the orifice. It is known that the length scale of the turbulence is inversely proportional to the strength of the eddy. In this case it follows that the flow behind the orifice probably has a stronger eddy structure near the wall due to the return of the flow to equilibrium.

Figure (33) shows a comparison between Eqs. (2) and (3). At intermediate separations $m/\delta^* \sim 2$, it is shown that the disturbed flow has a lower correlation than the basic flat-plate flow and suggests a considerable modification to the turbulence structure. For large separation distances the disturbed flow shows a higher level of correlation. This may be due to two different effects, but there is not sufficient evidence at this time to distinguish between them. On the one hand, if the cavity is resonating then the periodic pressure pulse would be an additive effect in the correlation causing the higher correlation at large separation. It can be noted that the geometry of the orifice suggests a resonance frequency of about 3,500 Hz. The other effect suggested may be the presence of a trailing vortex system downstream of the orifice which would retain its coherence for a considerable downstream distance and again increase the correlation for large separation distances. Since

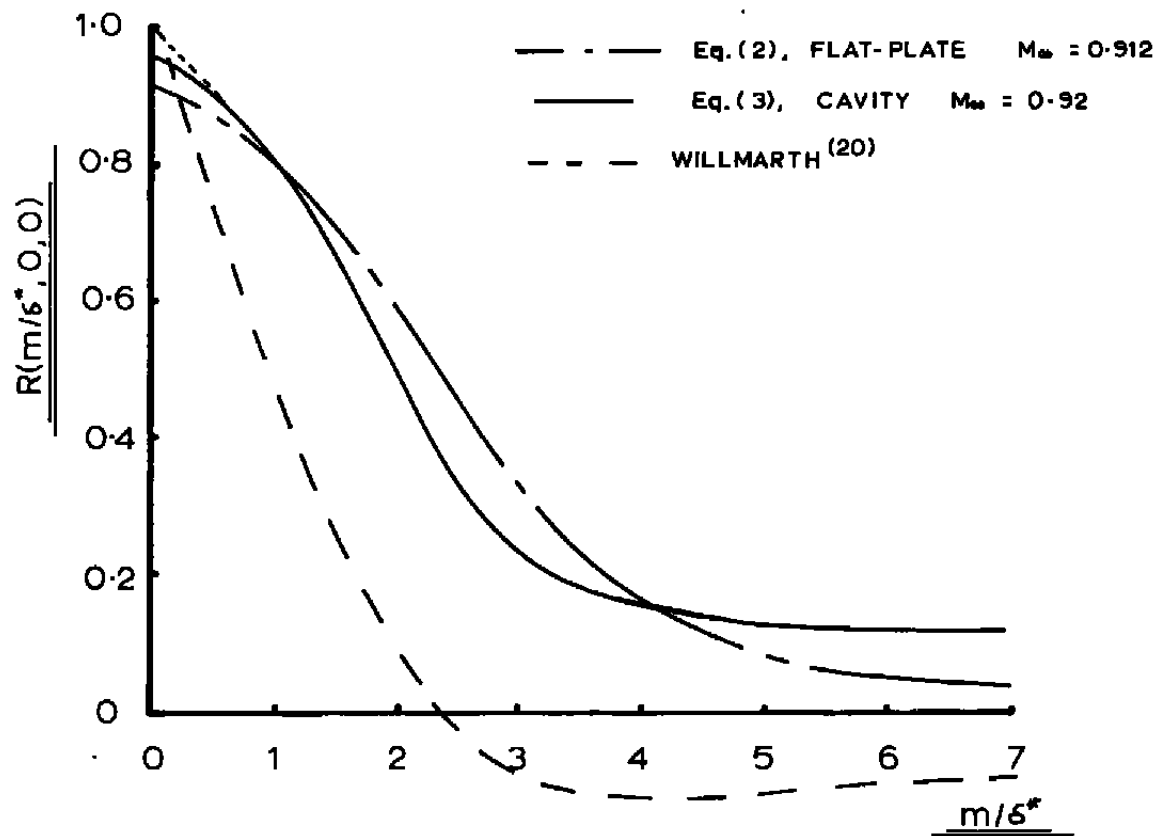


Figure 33. Comparison of Correlation Functions.

the surface oil flow study (Figure 24) does not define such a structure, further tests should be conducted to clarify this point.

Also included on Figure 33 is the data measured by Willmarth⁽²⁰⁾. There are two principle reasons for the differences between the correlation lengths in the two cases measured herein and that from Reference 20. First, there was no acceleration compensation applied to the present data and, as the correlation length for the vibration is likely to be large, this will have the effect of artificially increasing the correlation at the larger spatial separations, particularly.

Thus,

$$V_t = V_p + V_g$$

where V_t is total transducer millivolts
 V_p is millivolts from pressure
 V_g is millivolts from vibration

So,

$$\overline{V_t^2} = \overline{V_p^2} + 2 \overline{V_p V_g} + \overline{V_g^2}$$

but the correlation between pressure and vibration, $\overline{V_p V_g}$, is probably small. The second effect would be due to the rather high free stream turbulence level in the UTSI wind tunnel. For these reasons, the correlation function does not become negative in the present test (it may be noted that the AD531K is a four quadrant multiplier and would show negative correlation if this were present).

Both of these effects of vibration and free-stream turbulence will be essentially constant at a given run condition and should not destroy the comparison between the flat plate and the orifice flows as discussed above.

VII. GENERAL COMMENTS AND RELEVANCE OF STUDY

Many pertinent features of the orifice configuration have not been considered herein. Among these, particular mention should be made of orifice flushness and machining accuracy. Studies^(21,22) have shown the importance of these factors in the overall static pressure measurement and need not be repeated here. Due to the large diameter of the models used herein it is clear that any machining inadequacy is relatively less important than would be the case in actual application.

The present results are all for situations where the approach boundary layer thickness is of the same order as the diameter of the surface pressure orifice. It may be questioned as to how often such a situation occurs in practical model configurations. Figure 34 plots the variation of boundary layer thickness along a flat plate at a Mach number of one⁽²³⁾ and for three Reynolds numbers. A locus of points is shown for which the boundary layer thickness is 0.02 (i.e., equal to a typical orifice diameter).

In a favorable pressure gradient, or a laminar boundary layer, the boundary layer thickness would be smaller than this and the problem more severe. Also for a laminar boundary layer there is the possible transition tripping effect of the orifice.

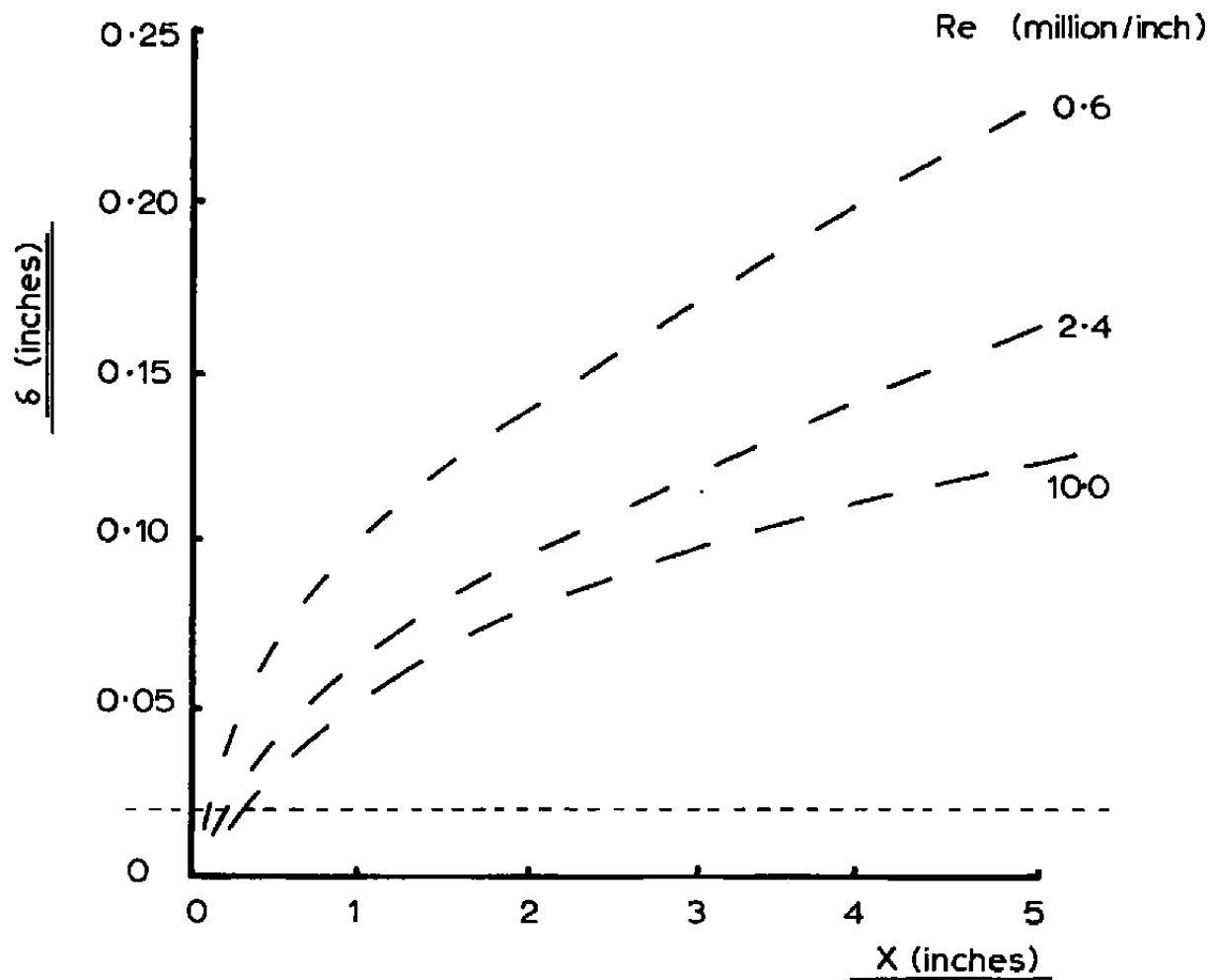


Figure 34. Calculated Boundary Layer Thickness as a function of Reynolds number at $M_\infty = 1.0$.

VIII. CONCLUDING STATEMENT

The present study has been concerned with the flow in and downstream of simulated surface static pressure orifices when the ratio of orifice diameter to approach boundary layer thickness is one or greater. As a result of the study it is possible to make several comments:

1. Particularly when the ratio of hole diameter to boundary layer thickness is greater than one then the boundary layer development downstream of the hole can be greatly modified. Close to the wall, this profile modification is restricted to a region directly downstream of the orifice with only a small spanwise spread. Directly behind the orifice, the major modification to the velocity profile is contained in the wall region. Then, as the flow returns to equilibrium, this profile distortion migrates out towards the edge of the boundary layer with a consequent increase in boundary layer thickness.
2. In general, the larger the ratio of hole depth to hole diameter the larger is the disturbance to the downstream boundary layer development. At the same time, the measurement error is reduced as this ratio increases beyond a value of about unity. These two trends appear to be in opposition so that some compromise must be made in the model design.

3. A full understanding of the flow mechanism by which the downstream boundary layer development is modified is not available. Certainly it is possible for resonance to take place in the hole under some conditions, but efforts to detect a strong radiation from the hole were not successful. Oil flow studies indicated that the flow was quite three-dimensional immediately downstream of the hole, with a strong demarkation from the 'undisturbed' flow.
4. The interaction between adjacent holes in a multi-hole model is complex and can, under some conditions, be a favorable interaction as far as the measurement error is concerned. This problem requires additional study.

The present study is not a complete evaluation of the problem but does serve to show the type of interactions that take place and indicates the need for additional work. Of greatest interest in this regard would be an in-depth study of multi-hole configurations.

The present results tend to show that the distortion to the downstream boundary layer is increased as the hole depth to diameter ratio is increased. A trend towards flush mounted miniature transducers would appear to be one long term solution to the problem of surface static pressure measurement.

REFERENCES

1. Wu, J. M., T. H. Moulden, G. M. Elfstrom, K. C. Reddy, C. H. Chen, R. Nygaard, L. Shen, H. H. Venghaus, and K. Anjaneyulu. "Fundamental Studies of Subsonic and Transonic Flow Separation, Part 1," AEDC TR-75-95, September 1975.
2. Shen, L. "On Transonic Wind Tunnel Design Considerations," Master's Thesis, The University of Tennessee Knoxville, 1974.
3. Hanley, R. D. "Effects of Transducer Flushness on Fluctuating Surface Pressure Measurement," AIAA Paper 75-534, 1975.
4. Plotkin, K. J. "Shock Wave Oscillation Driven by Turbulent Boundary Layer Fluctuations," AIAA J., Vol. 13, p. 1036, 1975.
5. Wieghardt, K. "Erhöhung des turbulenten Reibungswiderstandes durch Oberflächenstörungen," Tech. Berichte Band 10, Heft 9, 1943.
6. Ray, A. K. "Einfluss der bohrlochgrösse auf die Anzeige des statischen Druckes bei verschiedenen Reynoldszahlen," Ingenieur-Archiv, 24 (No. 3): 171-181, 1956.
7. Shaw, R. "The Influence of Hole Dimensions on Static Pressure Measurements," Journal of Fluid Mechanics, 7:550-564, April 1960.
8. Reed, T. D., Pope, T. C., and Cooksey, J. M. "Wind Tunnel Calibration Procedures Manual," Vought Corp., 1976.
9. Bradshaw, P., and F. Y. F. Wong. "The Reattachment and Relaxation of a Turbulent Shear Layer," Journal of Fluid Mechanics, 52:113-135, March 1972.
10. Kovasznay, L. S. G., Kibens, V., and Blackwelder, R. F. "Large Scale Motion in the Intermittent Region of the Turbulent Boundary Layer," JFM Vol. 41, 1970.
11. Kline, S. J., Reynolds, W. C., Schraub, F. A., and Runtstadler, P. W. "The Structure of Turbulent Boundary Layers," JFM Vol. 3, 1967.
12. McDonald, H., and Kreskovsky, J. P. "Effect of Free-Stream Turbulence on the Turbulent Boundary Layer," Int. J. Heat and Mass Transfer Vol. 17, 1974.

REFERENCES (Continued)

13. Krishnamurty, K. "Acoustic Radiation from Two-Dimensional Rectangular Cutouts in Aerodynamic Surfaces," NACA TN 3487, 1955.
14. Bitte, J., and Frost, W. "Analysis of Neutrally Stable Atmospheric Flow Over a Two-Dimensional Forward Facing Step," AIAA Paper 76-387.
15. Wu, C-I "Wall Pressure Fluctuations in the Turbulent Flow with Cavity Effect," M.S. Thesis, The University of Tennessee, 1976.
16. Hofland, R., and Glick, H. S. "A Miniature Transducer for Measuring Low Transient Pressures," Review Sci. Inst. Vol. 40, p. 1146, 1969.
17. Willmarth, W. W. "Structure of Turbulence in Boundary Layers," Advances in Applied Mechanics Vol. 15, Academic Press, 1975.
18. Bull, M. K., and Thomas, A. S. W. "High Frequency Wall Pressure Fluctuations in Turbulent Boundary Layers," Phys. Fluids, Vol. 19, p. 597, 1976.
19. Emmerling, R. "The Instantaneous Structure of the Wall Pressure under a Turbulent Boundary Layer Flow," Max-Planck Institut für Strömungsforschung Göttingen, 1973.
20. Willmarth, W. W., and C. S. Yang. "Wall Pressure Fluctuations Beneath Turbulent Boundary Layers on a Flat Plate and a Cylinder," J. of F. M., 41 (Part 1): 47-80, March 1970.
21. Franklin, R. E., and Wallace, J. M. "Absolute Measurement of Static-Hole Error Using Flush Transducers," J.F.M. Vol. 42, p. 33, 1970.
22. Rainbird, W. J. "Errors in Measurement of Mean Static Pressure of a Moving Fluid Due to Pressure Holes," Q. Bull. Mech. Eng. Nat. Res. Council, Canada, Rept. DME/NAE(3), 1967.
23. Nash, J. F. "A Practical Calculation Method for Compressible Turbulent Boundary Layers," Lockheed Georgia, ER-9428, 1967.

NOTATION

A_n	coefficients
b	distance, spanwise, from tunnel centerline
D	Diameter of pressure tube
d	orifice diameter
Hz	Hertz (K Hz - kilo Hertz)
h	orifice depth
k	constant
M_∞	free stream Mach number
M_e	Mach number at edge of boundary layer
m	spatial separation
n	index
P_t	total pressure
P	pressure (static)
P_∞	free stream static pressure
P'	pressure fluctuation
P_{mean}	mean pressure
q	dynamic pressure
R_e	Reynolds number/unit length
R_{e_δ}	Reynolds number based on boundary layer thickness
R_{e_H}	Reynolds number based on distance to orifice centerline
R	Correlation function
T_t	total temperature
t	time
u, v	velocity components along directions x, y
u_τ	friction velocity

NOTATION (Continued)

V_t	total transducer volts
V_p	transducer volts from pressure signal
V_g	transducer volts from acceleration signal
x'	x/d
x,y	coordinates along and normal to stream
δ	boundary layer thickness
δ_i	approach boundary layer thickness
δ^*	boundary layer displacement thickness
ΔP	pressure difference
μ	viscosity coefficient
ν	kinematic viscosity
τ	wall shear stress